Multi-level molecular modeling for plasma medicine

Annemie Bogaerts*, Narjes Khosravian, Jonas Van der Paal, Christof C. W. Verlackt, Maksudbek Yusupov, Balu Kamaraj and Erik C. Neyts

Research group PLASMANT, Department of Chemistry, University of Antwerp,
Universiteitsplein 1, BE-2610 Wilrijk-Antwerp, Belgium

*Corresponding author (annemie.bogaerts@uantwerpen.be)

Abstract

Modeling at the molecular or atomic scale can be very useful for obtaining a better insight in plasma medicine. This paper gives an overview of different atomic/molecular scale modeling approaches that can be used to study the direct interaction of plasma species with biomolecules or the consequences of these interactions for the biomolecules on a somewhat longer time-scale. These approaches include density functional theory (DFT), density functional based tight binding (DFTB), classical reactive and non-reactive molecular dynamics (MD) and united-atom or coarse-grained MD, as well as hybrid quantum mechanics/molecular mechanics (QM/MM) methods. Specific examples will be given for three important types of biomolecules, present in human cells, i.e., proteins, DNA and phospholipids found in the cell membrane. The results show that each of these modeling approaches has its specific strengths and limitations, and is particularly useful for certain applications. A multi-level approach is therefore most suitable for obtaining a global picture of the plasma-biomolecule interactions.

1. Introduction

In spite of the growing interest in plasma medicine for various applications, the underlying mechanisms at the atomic scale are not yet fully understood. One of the reasons is that the exact mechanisms are difficult to explore experimentally. Therefore, computer simulations can be very useful. There exist different atomic/molecular scale modeling approaches, which can be applied to study the interaction of plasma species with biomolecules or the subsequent behavior of these biomolecules as a result of such interactions. These methods range from very accurate but time-consuming quantum mechanical (QM) calculations, typically based on density functional theory (DFT), which can describe only very small systems, to more approximate classical (reactive or non-reactive) molecular dynamics (MD) simulations, which can handle much larger systems, and a variation or combination of the above methods, such as density functional tight binding (DFTB), quantum mechanical / molecular mechanics (QM/MM), united-atom or coarse-grained MD methods. A comprehensive review paper on atomic-scale modeling for plasma medicine, including some of the above methods, was recently presented in [1]. In the present paper, we will describe the entire spectrum of the above methods, applied to selected examples, which are important in the context of plasma medicine.

It is thus the purpose of this paper to give a broad overview of all currently employed methods, pointing out their strengths and weaknesses, in order to compare these methods. To illustrate this, we show an example for each of these methods. More detailed information on the methods and more extensive results for each of the examples, providing a better understanding of the interactions between ROS and

biological targets, will be presented in future papers. Furthermore, more information on the specifics of the methods used can also be found in specialized reviews, as indicated below.

In section 2, we will give a brief explanation of each of these methods. Depending on the application and kind of information that is envisaged, one or the other method is more suitable. This will be illustrated in section 3, where each of these modeling approaches is applied to specific model systems, relevant for plasma medicine applications. We selected three different types of biomolecules, which are present in the human cell, i.e., proteins, DNA and phospholipids in the cell membrane.

A plasma produces a cocktail of chemical species that may be important in plasma medicine, and depending on the type of plasma, also electric fields, ions or photons can play a role. Nevertheless, we focus here only on the interaction mechanisms of reactive oxygen species (ROS), which are known to play an important role in plasma therapy. More specifically, we focus on the interactions of OH radicals with these biomolecules, as well as the consequences of these interactions. We have indeed demonstrated before that other ROS, like O, HO_2, O_3 and H_2O_2, react more or less in the same way but are somewhat less reactive (except for O) [2-4], and moreover, we demonstrated that OH radicals are able to penetrate through a liquid layer surrounding biomolecules, while the O atoms rapidly form OH radicals upon reaction with H_2O molecules [5]. For this reason, the OH radicals are selected here as being representative for the ROS produced by the plasma.

In general, ROS can react with the cell membrane components (i.e., lipids and membrane proteins), as well as with biomolecules in the cell (e.g., DNA and proteins). They are able to oxidize lipids, proteins and DNA, and consequently damage these biomolecules or induce mutations in their structure. However, the underlying reaction mechanisms, as well as the consequences of these interactions, are not yet fully understood. In this paper, we will thus try to elucidate some of these mechanisms, by a combination of the various atomic/molecular scale simulation methods, described in section 2.

We want to stress, however, that these simulations cannot explain all underlying mechanisms in plasma medicine. Instead, their value lies in their capacity to elucidate the molecular level details of the first step processes. Plasma medicine is indeed much more complicated, due to the complex physiological and biological nature of living cells and tissues, involving also cell signaling and systemic reactions, which is clearly beyond the scope of the present type of simulations.

To validate this type of computer simulations, and to check whether they indeed might provide molecular-level insight, it would be interesting if experiments could be designed to provide molecular-level validation. This would be the first necessary step before the simulations can deal with real in vivo applications. For this purpose, very controlled conditions would have to be pursued, generating for instance only a beam of OH radicals instead of a complex mix of ROS and other plasma effects, and model systems of biomolecules, mimicking the more complex tissues. Such experiments have already been performed by several labs, investigating for instance the separate and synergistic effects of plasma-generated radicals and UV/VUV photons at the cellular and molecular level for various kinds of biomolecules, or experiments with simple model systems for the cell membrane, based on synthetic phospholipid membrane vesicles or liposomal model membranes (e.g., [6-16]).

2. Computational methods

The various computational methods that can be used to obtain atomic/molecular level insight in the interaction of plasma with biomolecular systems are illustrated in Figure 1, along with the corresponding system sizes and time scales that can nowadays standard be attained within a reasonable calculation time. It is clear that they cover a wide spectrum, from system sizes of about 100 atoms and picosecond

time scales, able to provide electronic structure information, up to system sizes of 10^8 atoms and time scales of microseconds, focusing on morphological information.

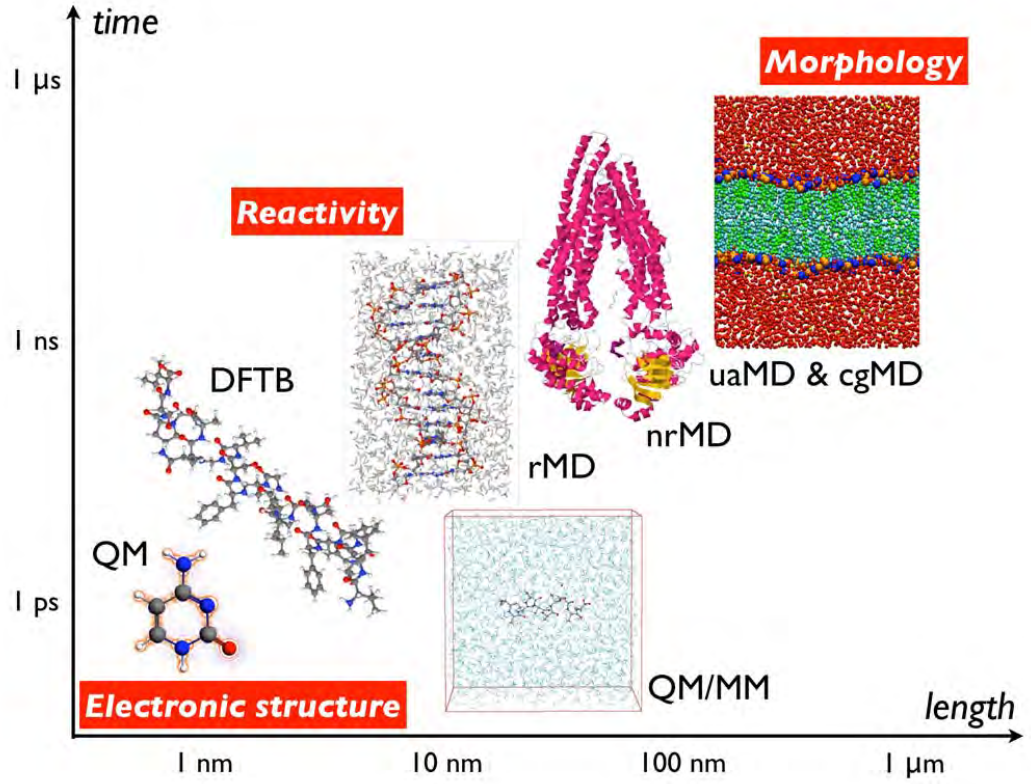

Figure 1: Overview of the computational methods that can be used for obtaining atomic/molecular scale insight in the interaction of plasma species with biomolecular systems, as a function of the attainable system sizes and time scales (QM = quantum mechanics, DFTB = density functional-tight binding, QM/MM = quantum mechanical / molecular mechanics, rMD = reactive molecular dynamics, nrMD = non-reactive MD, uaMD = united-atom MD, cgMD = coarse-grained MD).

2.1. DFT method

As mentioned above, the most accurate computational method is based on first principles, i.e., QM calculations. A very wide variety of QM techniques exist, varying in their approach to solve the Schrödinger equation and in the level of approximations made. Essentially, one can distinguish wave function-based methods, such as Hartree-Fock [17], Møller-Plesset perturbation theory [18], coupled cluster [19] or configuration interaction [20], from density functional theory (DFT) methods [21]. Especially in the field of plasma medicine, DFT seems more appropriate in view of the required system sizes. DFT relies on two fundamental theorems, proposed by Hohenberg and Kohn [22]. The first theorem states that the ground state energy from Schrödinger's equation is a unique functional of the electron density. This theorem allows to discard the enormous complexity of the wave function-based methods, since the wave function is a function of all 3N position variables (and in case spin is considered, also of N spin variables), while the electron density (and in case spin is considered, also the spin density) is a function of 3 position variables only. The second theorem states that the electron density, which minimizes the energy of the functional, is the true electron density. Hence, by

variationally minimizing the energy for the true functional, one (indirectly) solves the Schrödinger equation and has access to all system ground state properties. Unfortunately, however, the "true" functional is unknown, and various functional forms have been proposed. Typical examples of functionals include PW91 [23,24] and PBE [25,26]. More accurate results can be obtained with hybrid functionals, combining a portion of exact exchange from Hartree-Fock theory with exchange and correlation from, e.g., PBE or some other functional. A typical example is the B3LYP functional [27,28].

While highly accurate, DFT calculations are very time consuming. Standard system sizes that can be handled are typically in the order of 100 atoms. DFT-based MD calculations are also possible, and various schemes have been developed, including Born-Oppenheimer MD [29] and Car-Parrinello MD [30]. In these so-called ab initio MD (AIMD) methods, the accessible time scale is typically in the order of picoseconds.

To the best of our knowledge, there are currently no papers yet on the application of DFT calculations in the field of plasma medicine, although many DFT studies have been carried out for related systems and processes, including, e.g., amino acids and small peptides [31-34], DNA [35-37] and the cell membrane [38-40].

2.2. DFTB method

Somewhat larger systems can be handled with density functional tight binding (DFTB) methods. DFTB is an approximate DFT method, based on a Taylor series expansion of the DFT total energy expression [41,42]. The zeroth order approach of this method is equivalent to a standard non-self-consistent tight binding (TB) scheme [41]. For biomolecules, the second order approach (so-called "self-consistent charge DFTB", SCC-DFTB) is widely used [42-44]. It provides a reliable description of reaction energies and geometries of the structures studied, and the mean average deviations of the results from experimental values are comparable to DFT calculations [45]. This method has been augmented with an empirical treatment of the dispersion forces, to extend its ability to larger biomolecules [45,46]. It was tested for H-bonded complexes, small peptides, as well as DNA H-bonding interactions [47,48]. A still more extended and improved version of SCC-DFTB is the DFTB3 method [49]. It is derived from a third order expansion of the DFT total energy expression and it accurately describes the H-binding energies, proton affinities and proton transfer barriers without loss of speed and robustness. Typically, a few thousand atoms can be handled on time scales of tens of picoseconds. As is the case for DFT calculations, also DFTB calculations have so far not yet been applied to plasma medicine.

2.3. Classical reactive MD method

Up to now, atomic scale modeling for plasma medicine applications was mostly performed by means of classical reactive MD simulations [2-5,50-55]. In contrast to non-reactive MD simulations (see below), reactive MD simulations allow the description of bond breaking and formation, and thus they allow to study chemical reactions of plasma species with biomolecules. In a MD simulation, all atoms in the system are followed through space and time by integrating their equations of motion. Forces acting on the atoms are generally obtained as the derivative of some suitable interatomic potential, which is designed in such a way that bonds can break and form. This requires recalculating the bond order of each molecular bond at each time step during the integration. In classical MD, this potential is based on a large number of parameters, which can be obtained by fitting against DFT calculations. Examples of such reactive potentials are the Brenner potential [56] or the ReaxFF potential [57], which in the field of plasma medicine have successfully been applied to study for instance the reaction of ROS with peptidoglycan [2,3], lipid A [4], lipids [50-52], DNA [53,54], a water layer [5] and simple organic molecules in water [55]. Reactive MD simulations can typically handle much larger systems and much longer time scales compared to QM calculations, either at the DFT or the DFTB level. Depending on the

complexity of the interatomic potential, the number of atoms that can be handled is in the order of 10^4-10^6 at a time scale in the order of 1 ps – 100 ns.

2.4. Non-reactive MD method

While reactive classical MD is already much faster than QM calculations, they generally still require a long calculation time. In non-reactive MD simulations, the molecular connectivity in the system is fixed, such that the bond order of every bond does not need to be recalculated in every step. Therefore, this excludes the possibility of simulating bond formation and bond breaking, but it allows to simulate longer time scales. Often used non-reactive interatomic potentials (also called molecular mechanics (MM) force fields) include AMBER [58], CHARMM [59,60] and GROMOS [61,62]. The typically accessible system size and time scale is about two orders of magnitude larger than for reactive MD; hence, this method can handle in the order of 10^6-10^8 atoms, at a time scale in the order of 0.1 ns – 10 μs.

In the biomedical context, non-reactive MD simulations have mainly been applied to study the molecular mechanics of biomolecules (proteins, DNA,...), e.g., for drug designing purposes, to identify potential drug targets for several diseases [63-67].

2.5. United-atom and coarse-grained non-reactive MD method

Even longer time scales and larger system sizes can be handled by so-called united-atom and coarse-grained force fields. In a coarse-grained method, the atoms comprising entire functional groups are represented by coarse particles. Typically, 3-5 heavy atoms (i.e., non-hydrogen atoms) are grouped into one coarse-grained particle, allowing to reduce the number of particles in a system, which drastically speeds up the calculations. An example is the so-called Martini force field [68].

Furthermore, united-atom force fields (e.g., [69,70]) are intermediate between coarse-grained and all-atom force fields. In this case, all heavy atoms are treated separately, but the H atoms bound to a C atom will be treated as one (methyl or methylene) group, like in the case of the apolar tails of phospholipids (see section 3.6 below). Hence, the number of separate particles in the system is also reduced, but not so dramatically as in a coarse-grained method. Coarse-grained and united-atom MD simulations are generally non-reactive. The typical time scale and system size (in terms of number of particles) that can be handled are comparable to all-atom non-reactive MD simulations, but because individual atoms are grouped, the effective system size is typically up to one order of magnitude larger.

Systems and processes that can be handled in the field of biomedicine include, e.g., structural disintegration (and pore formation) of a phospholipid bilayer [71-75], protein-protein interactions [76-78], the behavior of double-stranded DNA [79,80] or carbohydrates [81,82].

2.6. QM/MM method

It is clear from above that each of these methods has its strengths and limitations, in terms of accuracy or type of information that can be obtained, as well as time scale and system size that can be handled (see also Figure 1 above). Very accurate methods, such as DFT, can only describe very small systems for short time scales, while non-reactive MD simulations can handle larger systems, but are not able to describe chemical reactions. However, these methods can also be combined, typically by handling a small and chemically the most relevant part of the system (e.g., the active site of the biological system) at the quantum chemical (electronic) level, and the surrounding embedding atoms and molecules at a classical (atomic) level. These simulations are often referred to as quantum mechanical / molecular mechanics (QM/MM) methods [83-85].

The QM/MM method enables to study chemical reactions at the quantum level, with a realistic and atomic description of the solvation environment. Two types of QM/MM techniques can be

distinguished, based on the level of the applied QM theory. The first type is based on semi-empirical methods, such as MNDO, AM1 [86], PM3 [87], empirical valence bond (EVB) [88], as well as the SCC-DFTB method [44], while the second type is based on ab initio methods, like wave function theory or DFT [89]. Ab initio QM calculations require more computation time than semi-empirical methods, but they are more accurate, and they have been widely used in a QM/MM setup, for investigating chemical and enzymatic reactions in biological systems. An overview of the applications of QM/MM in biomolecular systems was given in [90]. However, rigorous statistical mechanics sampling and reaction dynamics calculations remain a challenge, due to the high computational cost of the QM calculations.

3. Study of various biomolecular systems

In this section, we will illustrate how the above-described computational methods can be applied to study the interaction of ROS with various biomolecules, as well as the consequences of these interactions. As a first model system, we consider proteins. In section 3.1, we will show the principle of the QM/MM method to study the interaction of OH radicals with a simple peptide model system (i.e., deca-alanine). Furthermore, in section 3.2, the potential of DFTB simulations will be illustrated for the interaction of ROS (more specifically OH radicals) with P-glycoprotein. This is a transmembrane protein, which plays a crucial role in drug binding. The long-term behavior of this protein, as a result of the above interaction, will be described by non-reactive MD simulations in section 3.3. The second model system is DNA. In section 3.4, classical reactive MD simulations will be applied to study the interaction of ROS with a part of a DNA double helix. The third and last biomolecular system is the phospholipid bilayer (PLB), as a simple model system for the eukaryotic cell membrane. In section 3.5, the interaction of ROS with the PLB, leading to lipid peroxidation, will be studied with the DFTB method, and finally, in section 3.6, the further behavior of the PLB after lipid peroxidation will be illustrated with united-atom MD simulations. It must be noted that validation of the model predictions with experiments is not straightforward due to the limited time and length scales of these molecular level simulations. This makes a direct one-to-one comparison with literature not so easy. This type of simulations is mainly intended to provide some molecular-level insight, which is sometimes difficult to obtain by experiments.

3.1. Proteins: QM/MM study on deca-alanine peptide

(a) Computational details

The capabilities and limitations of the QM/MM method are illustrated for a very simple peptide model system, i.e., deca-alanine. More specifically, the reaction of an OH radical with alanine (Ala) at position 9 within deca-alanine is investigated. For this purpose, only the Ala residue at position 9 and the OH radical in the vicinity of this residue (see red circle in Figure 2b) are treated with the QM method, while the rest of deca-alanine and all water molecules surrounding this peptide are described by the classical MM method, using the Charmm 22 force field [91]. The QM/MM partition is made at the N-C bond connecting the Ala residues. So-called “link atom type” based on Integrated Molecular Orbital and Molecular Mechanics (IMOMM) [92] is applied to treat the boundary between the QM and MM regions. The QM subsystem is treated with DFT using the B3LYP functional and TZV2P basis set.

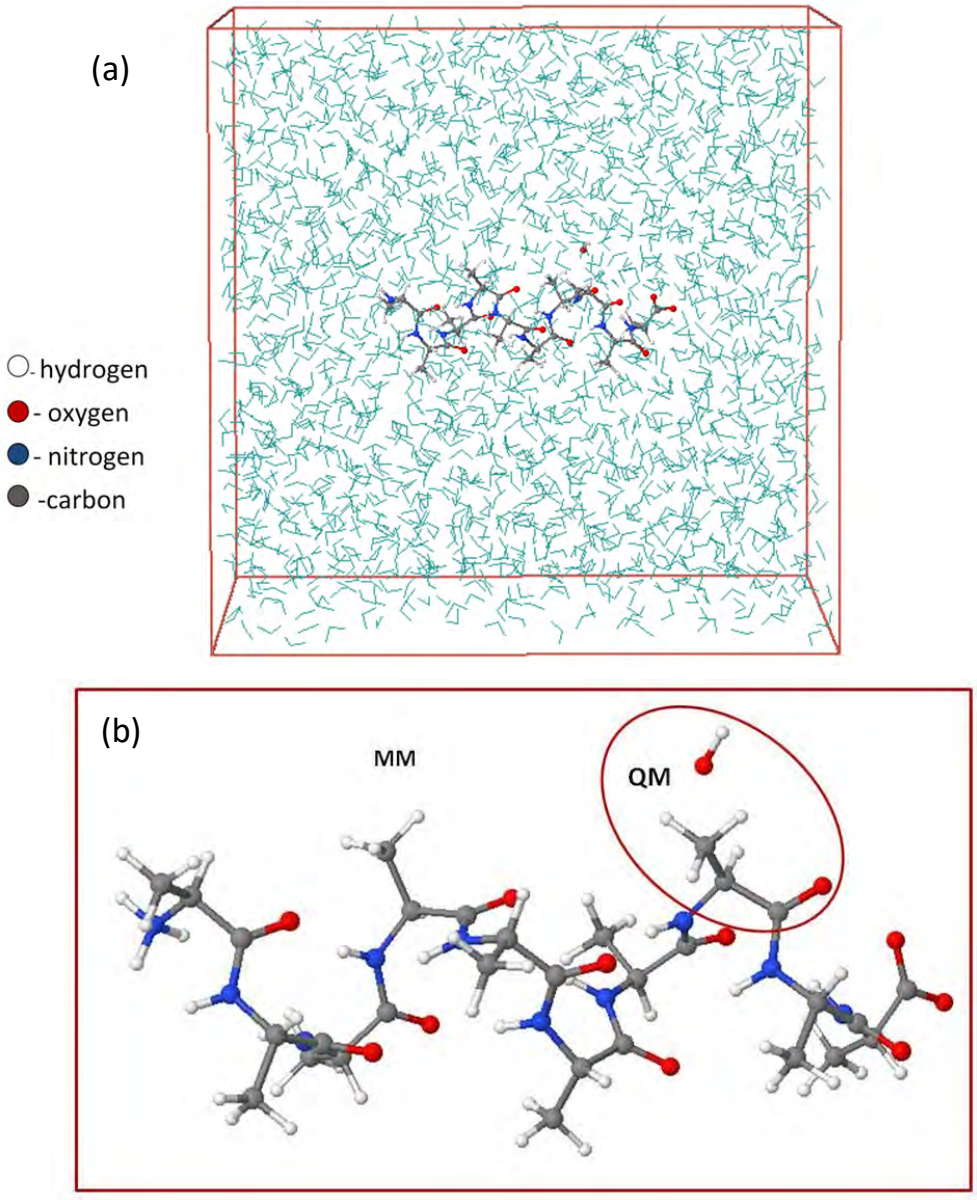

<u>Figure 2:</u> (a) Entire simulation box, containing deca-alanine, the OH radical and the surrounding water molecules (shown as blue sticks). (b) Part of the simulation box, illustrating the QM section and (part of the) MM section. For the sake of clarity, the water molecules are hidden here.

The simulation setup is as follows. Deca-alanine is located at the center of a box, filled with water molecules, with dimensions of 40Å × 40Å × 40Å (see Figure 2). The entire system is first minimized and then equilibrated based on the MM method at room temperature for 100 ps, by employing the Nosé-Hoover thermostat. The thermostat coupling parameter is set to 100 fs. After thermalizing the entire system with the MM method, DFT is applied in the QM partition, while the rest of the system is treated with MM, to equilibrate the QM/MM system in the NVT ensemble. The time step in this simulation is 0.5 fs.

<u>(b) Illustration of results</u>

In this particular example, the interaction of an OH radical with deca-alanine is studied. Our simulations indicate that the OH radical can indeed react with Ala in the QM subsystem and abstract the H_α atom. As a consequence, a water molecule is formed, and a C radical on deca-alanine is created, as shown In Figure 3. The C radical is highly reactive and can further react with another OH radical or other free ROS, yielding for instance peptide oxidation or even peptide bond cleavage. This peptide is of course only a simple model system, that does not occur in reality in human cells. Hence, this is just a simple illustration of the capabilities of the QM/MM method in the plasma medicine context. Applying the QM/MM approach in biological systems in the context of plasma medicine enables us to investigate the reaction of ROS with active sites of proteins, where substrate molecules bind and undergo a chemical reaction, as well as other potential fragmentation and oxidation sites of proteins.

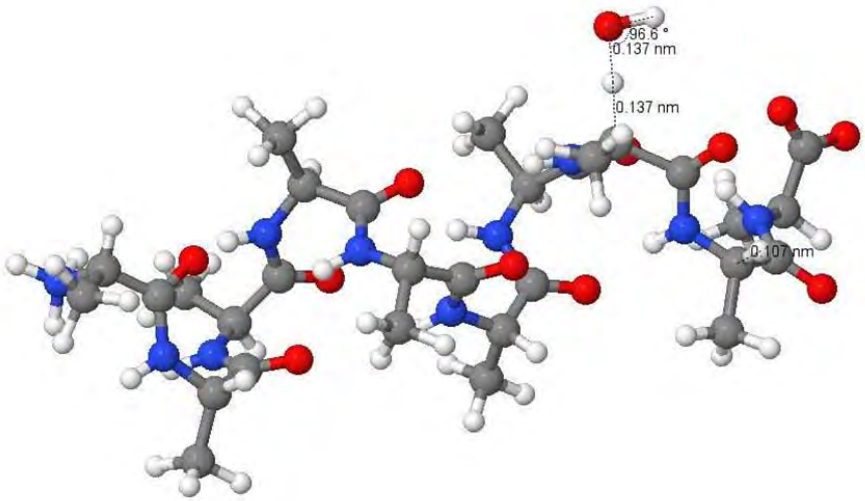

Figure 3: Snapshot from the QM/MM simulation, presenting the breaking of a C-H bond in the backbone of deca-alanine, due to OH impact on the H_α atom.

3.2. Proteins: DFTB study on P-glycoprotein

(a) Computational details

In this section, we present the interaction of OH radicals with P-glycoprotein, which is a very important protein, present in the plasma membrane of human cells. This protein is strongly expressed in tumor cells and causes reduced access of cytotoxic drugs in these cells [93]. Therefore, the multidrug resistance of cancer cells against chemotherapy is among others attributed to the function of P-glycoprotein [94]. This protein is composed of 1280 amino acids. It is known that transmembrane 6 (TM6) in P-glycoprotein plays a critical role in cytotoxic drug binding [95,96]. Therefore, in this study, we focus on the interaction of OH radicals with TM6 of P-glycoprotein, to elucidate the potential sites of fragmentation and mutation, and to obtain fundamental information about the underlying reaction mechanisms.

Our simulation setup is as follows. The TM6 structure is placed in the center of a simulation box with dimensions of 52Å × 27Å × 27Å. The structure of TM6 is shown in Figure 4. It is composed of valine (Val), leucine (Leu), thronine (Thr), phenylalaine (Phe), serine (Ser), isolucine (Ile), glycine (Gly), alanine (Ala), proline (Pro) and glutamine (Gln), in the following sequence: Val-Leu-Thr-Val-Phe-Phe-Ser-Val-Leu-Ile-Gly-Ala-Phe-Ser-Val-Gly-Gln-Ala-Ser-Pro-Ser-Ile (i.e., from position 331 to 352 in the P-glycoprotein

molecule). In total, the system contains 326 atoms. No surrounding water molecules were included in this case, to keep a reasonable calculation time. However, we focus on the interaction with OH radicals, which are known to be able to penetrate a water layer surrounding biomolecules [5], so the simulations should give a realistic outcome. Periodic boundary conditions are applied in all directions. The TM6 structure is first minimized and then equilibrated at room temperature by employing again the Nosé-Hoover thermostat. The thermostat coupling parameter is set to 100 fs. The steepest descent method is used for minimization with a maximum force component and SCC-tolerance equal to 10^{-4} and 10^{-5} a.u. (Hartree/Bohr), respectively.

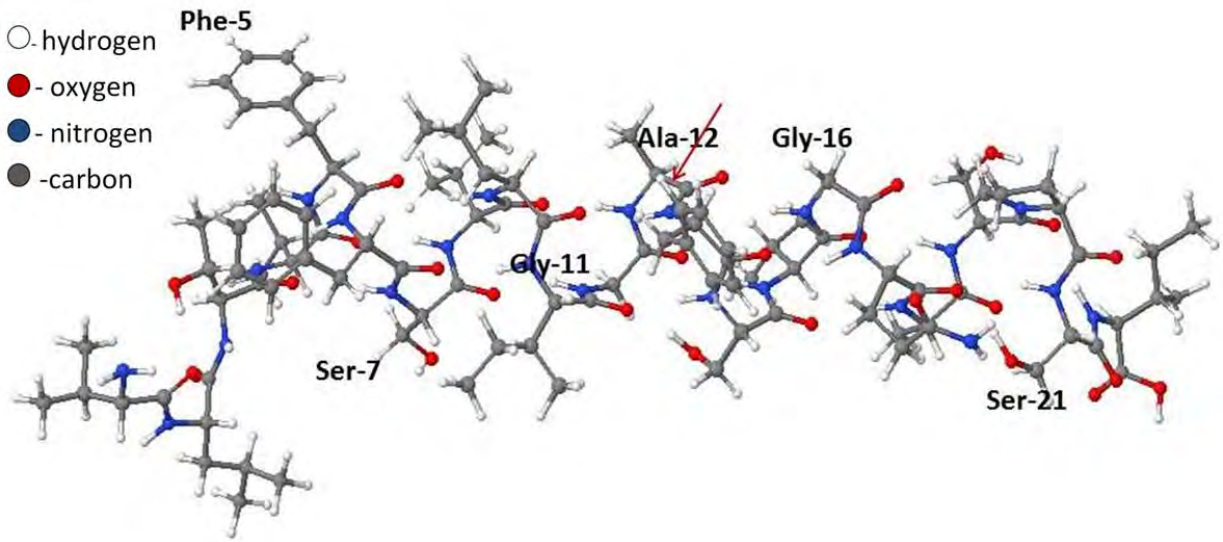

Figure 4: Structure of TM6, consisting of 22 amino acids. Some of the key residues (see below) are labeled. The red arrow line points towards the breaking of a C-C bond in Ala, leading to peptide fragmentation (see Figure 5 below).

To obtain statistically valid results for all reaction events, 50 simulation runs are performed. In each run, 10 OH radicals are initially randomly positioned at a distance of at least 5 Å around the TM6 structure and from each other, to avoid initial interactions between the impinging particles and TM6. The velocities are randomly chosen and correspond to room temperature. In all simulations (i.e., during equilibration and during particle impact), a time step of 0.5 fs is used. The total time per simulation is 10 ps.

(b) Illustration of results

We investigated all possible reactions in the backbone and side chains of TM6, leading typically to either oxidation, fragmentation and/or detachment of small molecules. Indeed, our simulations reveal that OH radicals can structurally damage TM6, through reactions in both the backbone and the side chains of the various amino acids within TM6.

In the backbone, the OH radicals can abstract the H_α of Thr, Phr, Ile, Ser, Leu, Pro, Ala, Val and Gly within TM6. The resulting C radical can react with other free OH radicals in the system, forming a new hydroxyl group on TM6 and initiating backbone oxidation and fragmentation. However, our results indicate that peptide bond cleavage was only observed in case of the interaction with Gly, Ser and Phe (corresponding to about 23% of all the reaction events).

Furthermore, the OH radicals are also able to react with all chemical groups in the side chains. The interaction of OH radicals with the hydroxyl group of Ser, Thr and Ile, and with the methyl group of Ala, as well as H-abstraction from the ring of Pro, gave rise to peptide bond cleavage (corresponding to about 78% of all reaction events), while the other reactions only lead to the detachment of some small (hydrocarbon or aldehyde) molecules, or peptide oxidation.

The mechanism of peptide bond cleavage upon impact of an OH radical on the methyl group of Ala at position 12 is illustrated in Figure 5. For clarity, the relevant atoms are numbered. An OH radical (O_1) abstracts the α-hydrogen (H_2) of Ala, forming a water molecule (red circle in (a-b)). The remaining carbon radical (C_3) attempts to share an electron with C_4, forming a C_3=C_4 double bond. As a consequence, the C_4-C_5 bond breaks up (c). So, fragmentation in TM6 due to the breaking of a C-C bond in Ala occurs (pointed out by the red arrow line in Figure 4).

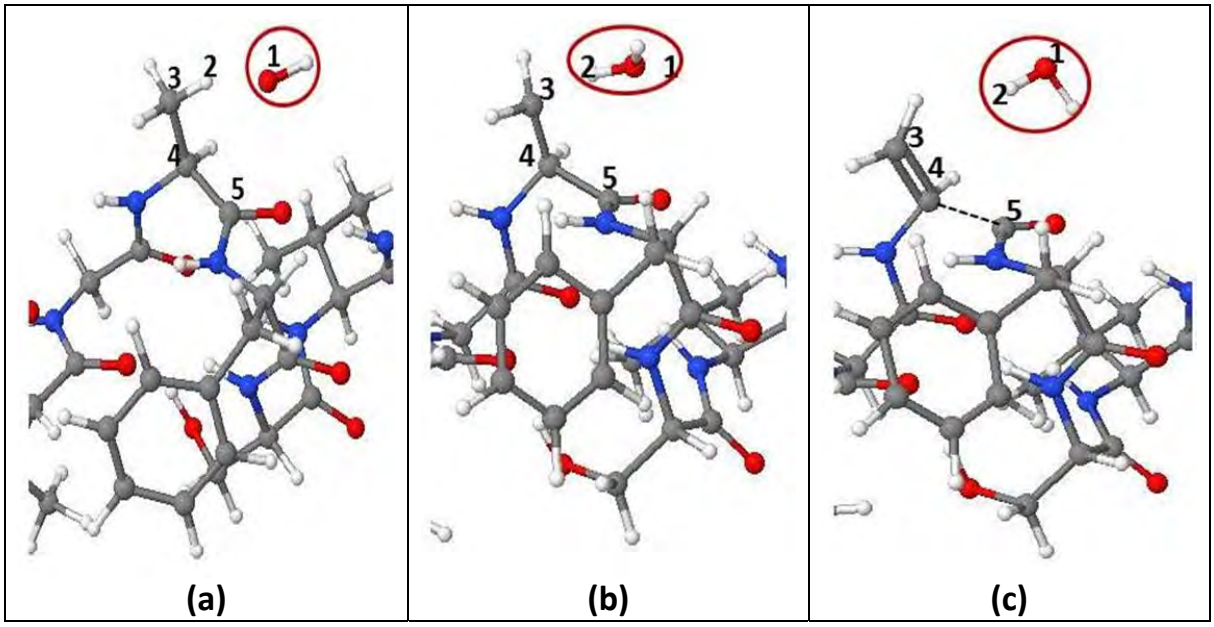

Figure 5: Snapshots from DFTB simulations, presenting the breaking of a C–C bond in the backbone of TM6 upon OH impact on the methyl group of Ala. (a) OH (red circle) first approaches H of the methyl group. (b) OH abstracts H_2 connected to C_3, forming a water molecule (red circle). (c) A double C_3=C_4 bond is created, leading to dissociation of the C_4-C_5 bond (see black dashed line).

Finally, the OH radicals can also interact with the aromatic ring of Phe, yielding either OH addition or H abstraction, resulting in a change of the aromaticity of the Phe ring, which will lead to a different binding energy with the drugs. Moreover, when OH addition and H-abstraction occur at the same position in the ring, which occurred 8 times in our simulations (i.e., 500 OH radical impacts), a new amino acid, i.e., Tyr, will be formed. This process is depicted in Figure 6. The OH radical forms a bond with C_2 in the para site of the aromatic ring (a). Another OH radical abstracts the H_4 atom on this para site (b), forming again a water molecule, while Phe is converted into Tyr. The same product is also experimentally observed in the hydroxylation of Phe by the Fenton reaction and γ-radiolysis [97]. As the binding of cytotoxic drugs with P-glycoprotein mainly occurs with the aromatic ring of Phe in TM6 (see above), this mutation might affect the response of the human cell in cancer therapy. Indeed, the overexpression of P-glycoprotein leads to a multidrug (vinblastine, verapamil, colchicine,…) resistance phenotype in various forms of

cancer, which is a major barrier to the successful treatment of cancer [94]. Our predictions of this mutation might contribute to a better understanding for this drug resistance problem, as was also demonstrated already in literature for another mutation of Phe at the same position in P-glycoprotein [96]. Hence, we believe that this might be important for plasma cancer therapy (or other therapies based on ROS), to reduce the multidrug resistance in combination with classical chemotherapy, as has already been demonstrated experimentally [98]. However, more direct experimental evidence for the effect of this mutation on drug resistance will be needed, before we can really draw conclusions.

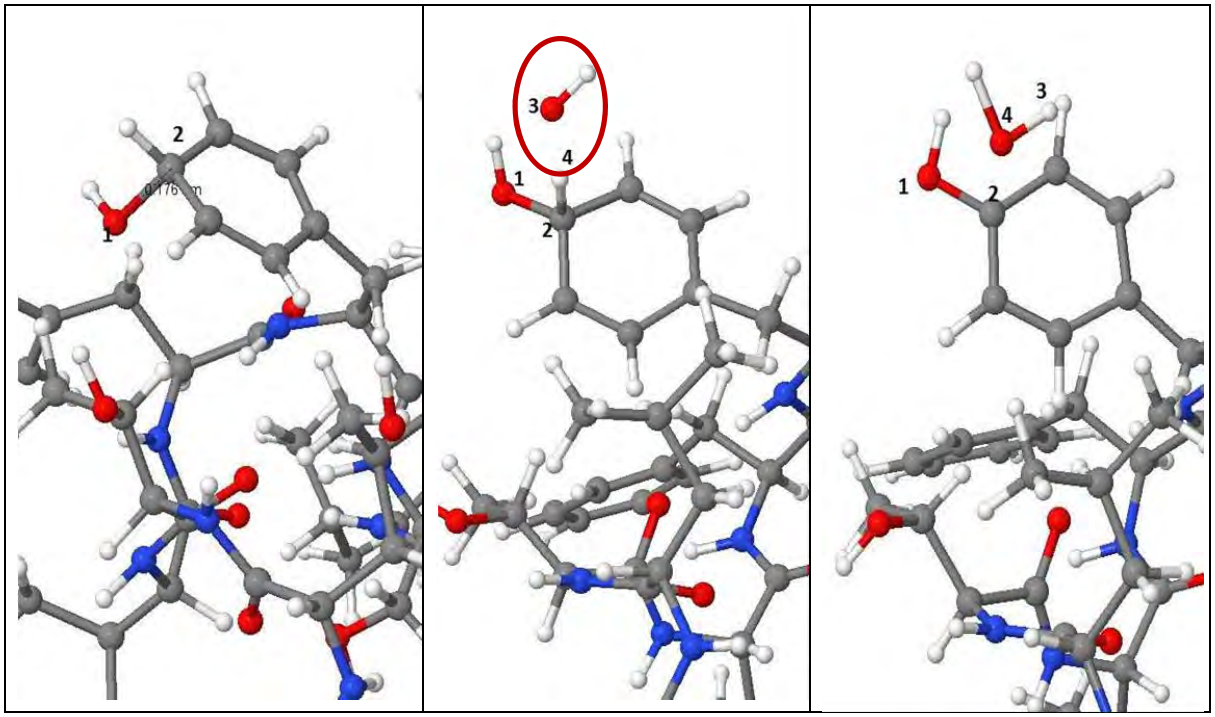

Figure 6: Snapshot from DFTB simulations, illustrating the mutation of Phe into Tyr, upon impact of an OH radical on the aromatic ring of Phe in TM6. (a) OH attaches to the para site of the aromatic ring. (b) Another OH radical approaches the H_4 atom of this para site (red circle). (c) H_4 is abstracted by the OH radical, converting Phe into Tyr.

3.3. Proteins: Non-reactive MD study on P-glycoprotein

(a) Computational details

To study the structural behavior of TM6 upon mutation of Phe into Tyr, with implications for drug binding, we also apply non-reactive MD simulations, using the GROMACS 4.6.3 package [99]. Indeed, these simulations are less computationally demanding, and thus able to handle longer timescales, needed for this purpose.

More specifically, we performed non-reactive MD simulations for the native structure of TM6, as well as the mutant structure upon OH impact. This mutation is called F335Y, because phenylalanine (F) at position 335 within TM6 is converted into Tyrosine (Y); see previous section. The systems were solvated in a cubic box with SPC water molecules. The whole molecular system was first subjected to energy minimization by the steepest descent algorithm, implementing the CHARMM27 all-atom force field.

Subsequently, the minimized systems were subjected to MD simulations. The Particle Mesh Ewald (PME) method [100] was used to treat the long-range electrostatic interactions. We analyzed the root mean square deviations (RMSD), the define secondary structure of proteins (DSSP), the helicity and the root mean square fluctuations (RMSF) and we applied principal component analysis (PCA), for both the native and mutant structure, to examine the structural and functional behavior of TM6 of P-glycoprotein.

(b) Illustration of results

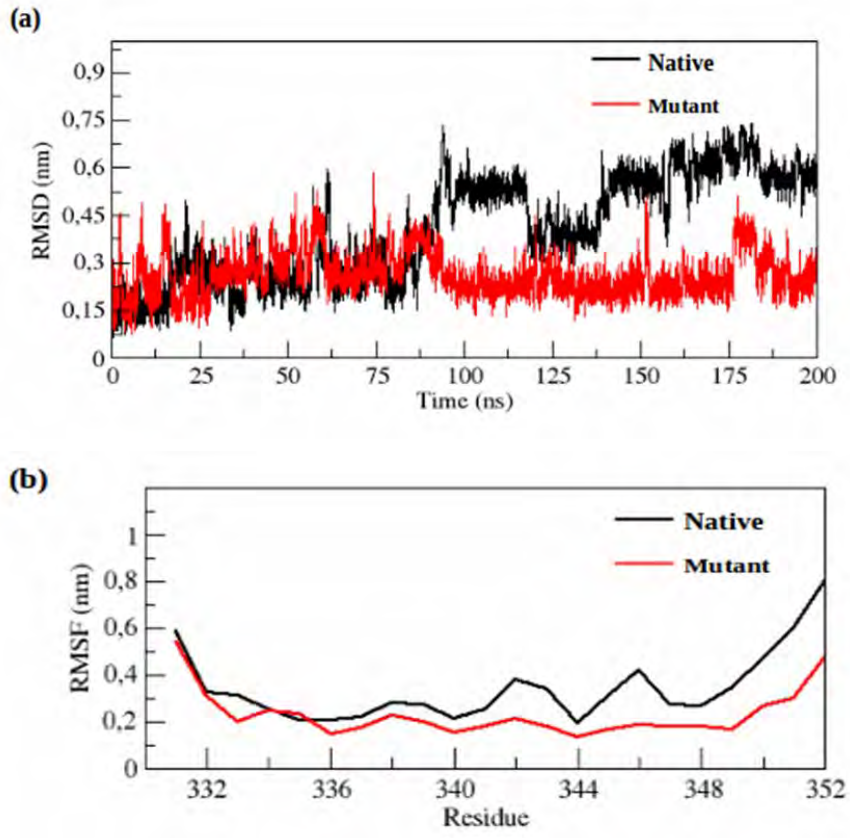

Figure 7: RMSD vs time (a) and RMSF (b) of C_α atoms of native and mutant TM6 of P-glycoprotein at 300 K.

In Figure 7(a), we plot the RMSD for all C_α atoms of the native and mutant structure of TM6. It is clear that the native and mutant structures show a similar deviation until ~89 ns, but then the native structure starts deviating more than the mutant structure. The average RMSD values of the native and mutant structures over the simulation time are 0.41 ± 0.16 nm and 0.26 ±0.07 nm, respectively. This indicates that the native structure is more flexible, while the mutant structure becomes more rigid. The same can be deduced from the RMSF plot, presented in Figure 7(b). Indeed, the mutant structure shows a somewhat lower degree of flexibility than the native structure, which is most apparent in residues 336-352 in Figure 7(b). The average RMSF values of the native and mutant structures over the simulation time are 0.34 ± 0.15 nm and 0.23 ± 0.10 nm, respectively. Furthermore, also the DSSP (showing the secondary structural conformation of TM6) and the helicity fraction were analyzed (not shown), and again confirm that the mutant structure has a larger fraction in α-helix conformation, pointing out the higher rigidity than the native structure. Finally, the projection of the first two

eigenvectors as obtained from the PCA (see Figure 8) shows that the mutant structure covers a smaller region of phase space in both the PC1 and PC2 plane than the native structure, again indicating that it has lost its flexibility and has become more rigid in structure. This might affect its conformation, which may increase the drug binding affinity with P-glycoprotein. However, more investigations are needed to draw final conclusions.

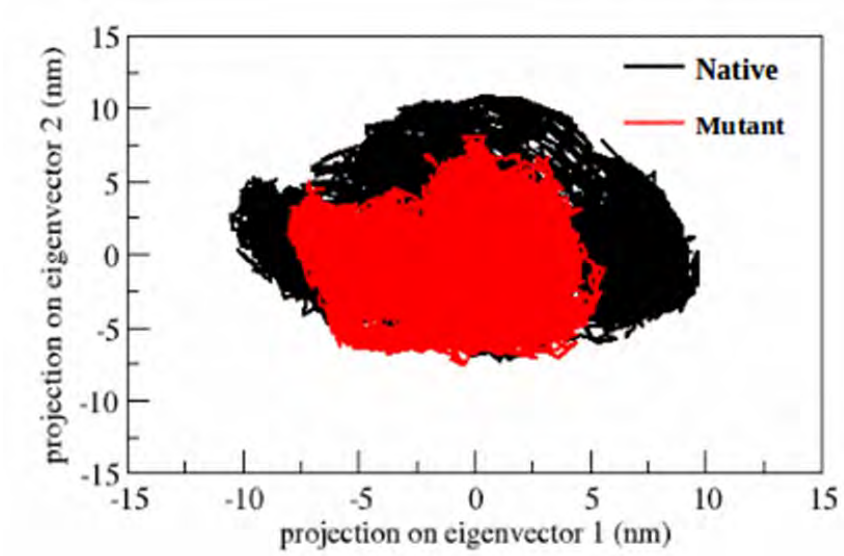

Figure 8: Projected motion of TM6 of P-glycoprotein in phase space along the first two principal eigenvectors at 300K.

3.4. DNA: Classical reactive MD study

(a) Computational details

In case of the interaction of ROS with DNA, we applied classical reactive MD simulations, using the ReaxFF force field [57]. This method has the advantage of being able to describe bond breaking and formation, and thus chemical reactions, on relatively large systems, compared to the DFT and DFTB methods.

ReaxFF is a classical force field, employing in the order of 100 parameters, optimized against QM data. It is one of the most widely parametrized and accurate reactive force fields currently available, with an accuracy for hydrocarbons stated to be similar to or better than semi-empirical QM calculations at the PM3 level, while being 100 times faster [57]. In ReaxFF, the total potential energy of the system is the sum of multiple partial energy contributions, including bond energy, valence and torsion angles, over- and undercoordination corrections, conjugation terms and the non-bonded van der Waals and Coulomb interactions. A number of different parametrizations have been developed and optimized for ReaxFF, for different systems. In this study, we make use of a modified version of the force field developed by Monti [101], containing parameters for C/H/O/N/P atoms.

Although the classical MD method is less time-consuming than DFT and DFTB, it is still limited to relatively small structures (order of a few 10,000 atoms). As DNA is an extremely large molecule, it is thus impossible to model it as a whole, hence we selected some representative fragments, containing 12 base pairs, surrounded by water molecules, as a model system (see Figure 9). We focus here again on the interaction of OH radicals with DNA, as the O atoms from the plasma would be converted into OH

radicals when traveling through the liquid phase before reaching the DNA molecule [5], and the other ROS were found to be significantly less reactive.

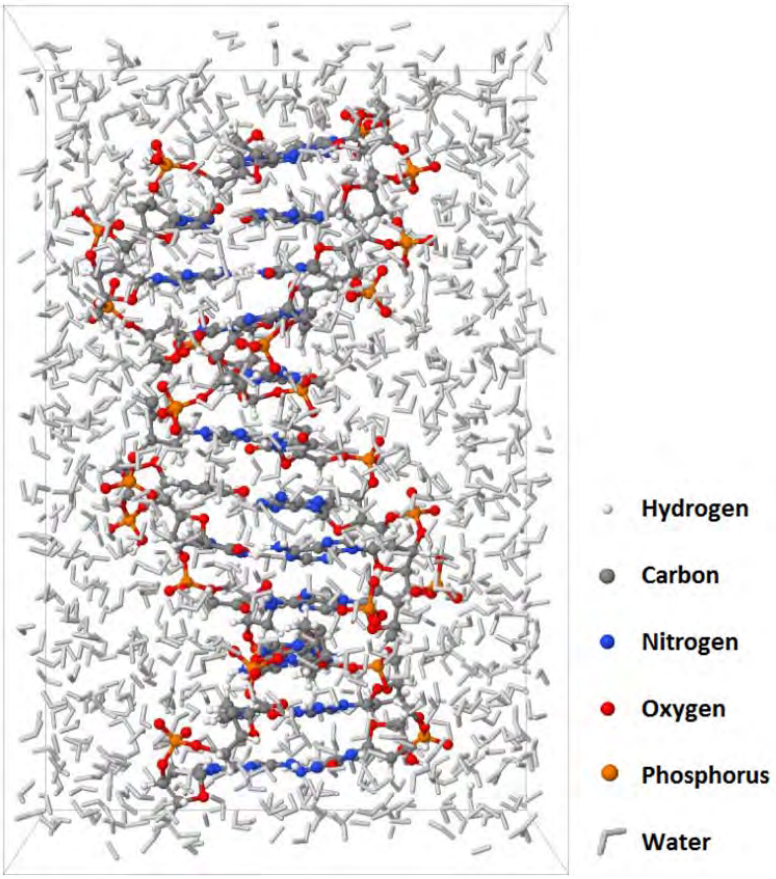

Figure 9: Snapshot of the 12-base-pair DNA double helix in water, used for the reactive MD simulations.

A DNA string is placed in a rectangular simulation box, with dimensions of 33Å x 33Å x 48Å. The remaining volume of the simulation box is filled with water molecules (approaching a density of 1 g/ml), providing a simple model for DNA found in the nucleoplasma/cytosol of living cells. The simulation box is periodic in all three dimensions. As the force field only describes interactions among C/H/O/N/P atoms, no additional atoms were included (e.g., counter ions for the negative phosphate groups).

Before starting the simulations of the OH interactions with the DNA molecule, the system is equilibrated at room temperature for 300 ps in the canonical ensemble (NVT) using a Nosé-Hoover thermostat with coupling constant of 25.0 fs. Subsequently, 10OH radicals are randomly placed around the DNA molecule, to investigate their interaction mechanisms. 15 impact simulations are performed, to obtain some (limited) statistics about the occurring processes. The simulations are carried out for 500 ps, to allow enough time for reactions to occur, while still keeping the simulation time reasonable.

(b) Illustration of results

Mainly two types of reactions are observed, i.e., (i) H-abstraction from a (primary or secondary) amine in the nucleic bases and (ii) the addition of an OH radical on the purine ring of the nucleic bases. The H-abstractions from the amines result in a radical that can lead to some more (intermolecular) H-

abstractions. As these H atoms are often part of the H-bridge structure between the two DNA strands, it is well possible that they affect the H-bridge system.

The OH-addition on the purine ring of the nucleic bases, more specifically at the C-8' position of dAMP and dGMP, results in the formation of 8-hydroxy-purine adduct radicals (8-OH-Ade$^{\bullet}$ or 8-OH-Gua$^{\bullet}$). This is illustrated in Figure 10 for dGMP. This reaction is the first step towards the formation of 8-oxo-guanine (8-O-Gua) and 2,6-diamino-4-hydroxy-5-formamidopyrimidine (FapydG) [102], which are known as markers for oxidative stress in cells [102-104]. The introduction of these products may have a devastating effect on the biochemical pathways within the affected cells, e.g., introduction of DNA mutations or inhibition of gene expressions, which might possibly lead to apoptosis. These further reactions could, however, not be observed in our simulations, due to the limited calculation time.

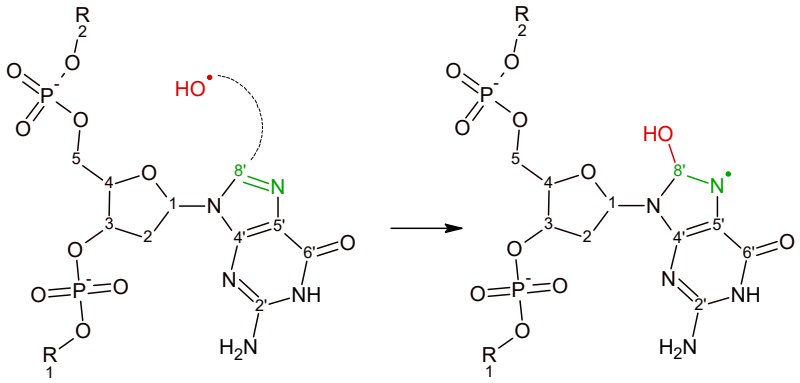

Figure 10: Schematic illustration of the OH-addition on C-8' of DGP, resulting in the formation of an 8-OH-guanine adduct radical. R1 and R2 correspond to the preceeding and following nucleotides.

In addition to the above-mentioned reactions, a strong affinity between OH radicals and the C-5 position on the backbone has been observed. This is very important, as it points towards a possible pathway for the formation of single strand breaks (SSBs). It is known that SSBs are initiated by H-abstraction reactions on C-H bonds of the backbone ribose (preferably at the C-4 or C-5 position, see figure 10 for the numbering). The resulting radicals will either react with surrounding oxygen species (e.g., O_2) or lead to a direct breaking of the phosphodiester bond, both resulting in SSBs. Furthermore, when combined with a second SSB at the opposite strand in close vicinity, this might result in a double strand break (DSB), cleaving the DNA double helix, which activates pro-apoptotic factors. As stated in literature [105], when both strands are broken within 20-57 base pairs by SSBs, DSB will eventually occur when enough H-bridges between both helices are broken. Our simulations reveal that a loose DNA strand end can migrate away from the complementary strand, breaking the H-bridge system over time, as illustrated in Figure 11. Although the simulated end points are inherent to the simulation setup and do not occur in reality, the same is expected to happen with the nucleotides at the positions of SSB. Indeed, the H-bridges between these nucleotides are replaced with H-bridges with the water molecules, slowly opening the DNA helix (see bottom base pair in the right snapshot of Figure 11). As a result of this migration of nucleotides in solution, more oxidation reactions might occur at these positions, which might be difficult to repair. We expect that for longer simulation times, more and more H-brides between opposite nucleic basis will be replaced by H-bridges with water molecules, so that two SSBs in the vicinity of each other might eventually lead to DSBs. More details about these simulations can be found in [106].

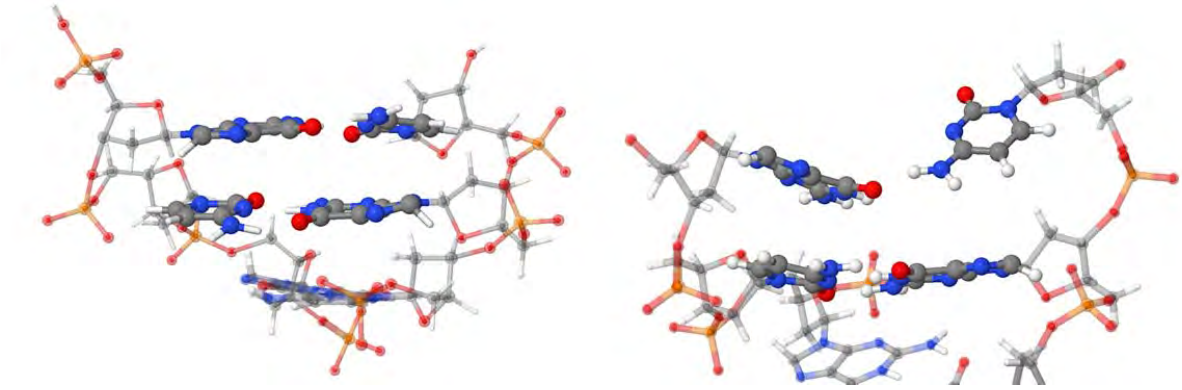

Figure 11: Snapshots of the DNA break, before (left) and after (right) the impact simulations, depicting the partial opening of the DNA double helix. In the right snapshot, a drop in interstrand H-bonds can be deduced at the top nucleotide pair, keeping only the H-bond between dGMP-O and H-dCMP. For the sake of clarity, only the top three nucleotide base pairs of the dodecamer are shown, and the backbone and last base pair are depicted with semi-transparent and thinner ball-and-stick model. The color code is identical to Figure 9. As the structure on the right was found on the periodic border of the simulation box, the top-most phosphate group, of the left snapshot, is not visible in this snapshot.

3.5. Phospholipid bilayer: DFTB study

(a) Computational details

Our model system for the phospholipid bilayer (PLB), studied with the DFTB method, consists of phosphatidylcholine molecules, i.e., one of the four main phospholipids (PLs) found in mammalian cells and most abundant in the cell membrane [107]. Specifically, we consider 1-palmitoyl-2-oleoyl-*sn*-glycero-3-phosphocholine (POPC) presented in Figure 12(a).

It has a hydrophilic head group (i.e., the choline, phosphate and glycerol groups in Figure 12(a)), containing two hydrophobic fatty acid tails (i.e., palmitoyl and oleoyl in Figure 12(a)). One of the tails (i.e., oleoyl) contains one double (unsaturated) C=C bond, whereas the other (i.e., palmitoyl) remains fully saturated.

The PLB structure under study is composed of 8 PL molecules, with water layers on top and at the bottom (see Figure 12(b)), that are placed in a box with dimensions of ~ 16Å × 72Å × 18Å. The geometry of the structure is optimized using the conjugate gradient algorithm. The system is then equilibrated for 5 ps (i.e., 10^4 iterations) in the isothermal-isobaric ensemble, following NPT dynamics (i.e., constant number of particles, pressure and temperature) at 300 K, employing the Berendsen thermostat and barostat [108] with a coupling constant of 100 fs and 700 fs, respectively. In all simulations (i.e., during the thermalization, as well as during the particle impact simulations) we use a time step of 0.5 fs. Periodic boundary conditions are applied in all three directions to mimic the infinity of the system. The impacts of the ROS are then simulated by the MD method, for 5 ps (i.e., 10^4 iterations).

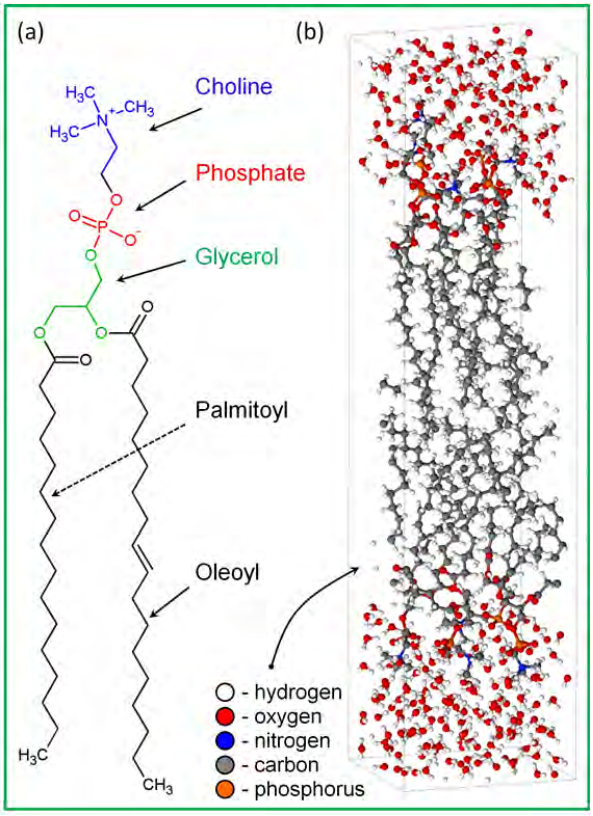

<u>Figure 12:</u> Schematic picture of the POPC molecule (a) and the PLB to be treated with the DFTB method (b). The PLB in (b) consists of 8 PL molecules, i.e., 4 PLs (with water layer) at the top and 4 at the bottom.

We illustrate here the interaction of the ROS, formed in the plasma, with the head groups of the PLB, and not with the lipid tails, as it is already well established from experimental studies (e.g., [109-111]) which (per)oxidation products of the lipid tails are formed, while much less is known about the products formed by interaction with the head groups. Moreover, it was revealed from free energy profiles for the translocation of various ROS across a POPC bilayer, that OH, HO_2 and H_2O_2 species preferably stay closer to the head group of the PLB [112].

The ROS under study, i.e. O, O_3, OH, HO_2 and H_2O_2, first have to penetrate the water layer before reaching the head group of the PLB. Our simulations reveal that O_3, HO_2 and H_2O_2 exhibit no bond breaking events with water, so these species can freely move through the water layer. The O atoms, on the other hand, react with water molecules, leading to the formation of two OH radicals. These two OH radicals can react with each other, forming a H_2O_2 molecule, or they can also react with water, exchanging a H atom and forming again the same species (i.e., forming a new OH radical and a water molecule), a process which is continuously repeated. The behavior of the ROS in a liquid layer was studied in detail in our previous work for O, OH, HO_2 and H_2O_2 by means of classical reactive MD simulations [5], and roughly the same behavior is also predicted with our DFTB method. We can thus conclude that all of the ROS investigated, except for the O atoms, are in principle able to react with the head group of the PLB, after travelling through the water layer.

Upon interaction with the head group of the PLB, our simulations reveal that HO_2, H_2O_2 and O_3 molecules do not react with the head group, and they only show weak attractive non-bonded interactions with the structure.

In the case of OH radicals, we do observe reactions with the head group of the PLB, leading to the cleavage (or formation) of some bonds. Several reaction mechanisms are observed, and they are all initiated by H-abstraction from (different parts of) the head group, but not all of them give rise to further bond breaking. We will focus here on the mechanisms that lead to the detachment of some parts in the PLB, which is important for the long term behavior of the PLB (see also next section). One of these interaction mechanisms is illustrated in Figure 13.

The OH radical first abstracts a H atom from the methyl group of choline (see Figure 13(a-b)) forming a water molecule. This leads to the formation of a double C_1=N bond and the breaking of the C_2-N bond (see Figure 13(c)), and thus to the detachment of the NC_3H_8 group, as well as the creation of a dangling bond at C_2. Subsequently, a new OH radical can either react with this C_2 radical and form an hydroxyl group (see Figure 13(d)), or abstract a H atom from the CH_2 group positioned beneath this C_2 radical, forming a stable double C_2=C_3 bond (see Figure 13(e)). We checked which of these two reactions is energetically more favorable, by means of DFT calculations, using the B3LYP functional [113] with the Slater-type basis set TZ2P [114]. The calculated reaction energies of these two reactions reveal that the first reaction (i.e., the formation of the alcohol group) is energetically slightly more favorable.

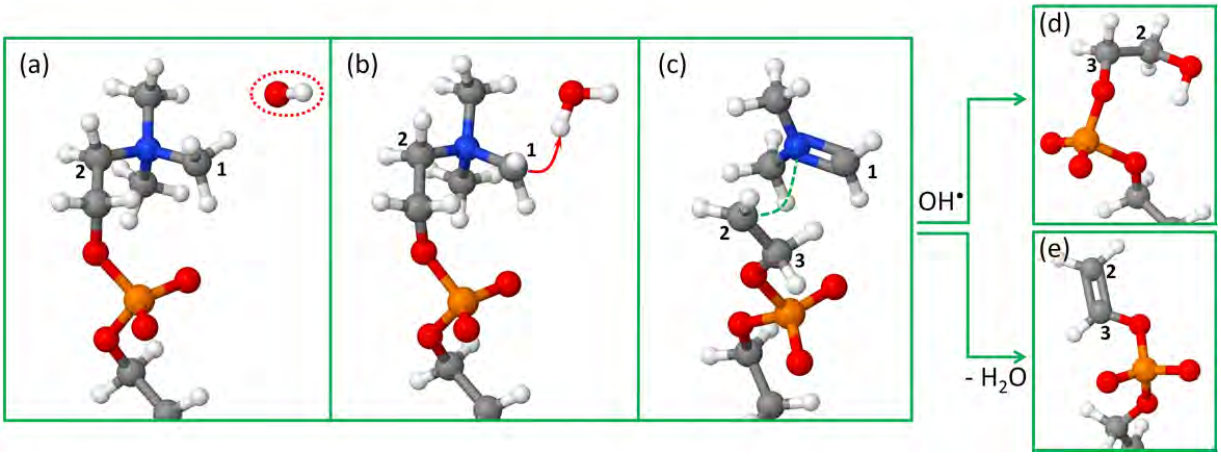

Figure 13: Snapshots from the DFTB-MD simulations, showing the interaction of an OH radical reacting with the choline group of the POPC molecule (cf. Figure 12(a)), leading to the dissociation of a C-N bond and the detachment of the NC_3H_8 group. The OH radical (shown in red dashed circle) approaches the choline (a), and abstracts a H atom connected to C_1, leading to the formation of a water molecule (b). This results in the formation of a double C_1=N bond and dissociation of the C_2-N bond (c). The H-abstraction and the dissociation of the bond are indicated in the figure with a red arrow and a green dashed line, respectively. Subsequently, two mechanisms can occur: a new OH radical can react with the C_2 radical, forming a hydroxyl group (d), or this OH radical can abstract the H atom from the adjacent CH_2 group (i.e., the H atom bonded to C_3), forming a double C_2=C_3 bond (e).The color legend is identical to Figure 12.

The detachment of the NC_3H_8 group might change the polarity (or hydrophilicity) of the head group, and likewise, the hydrophobicity of the lipid tails can also be changed due to the migration of this NC_3H_8 group towards the lipid tails. These subsequent processes happen on a longer time scale, and can thus

not be studied with the DFTB method, but they can be investigated with the united-atom non-reactive MD method, an example of which will be illustrated in section 3.6 below.

Another mechanism that can occur upon impact of OH radicals on the head groups of the PLB is depicted in Figure 14. After the H-abstraction from CH_2 of glycerol (see Figure 14(a-b)), a water molecule and a double C_1=C_2 bond are formed, followed by the detachment of the whole oleoyl chain (see Figure 14(c)). Subsequently, the detachment of a CO_2 molecule occurs from this chain (not shown in Figure 14), leaving behind a radical site. A new OH radical can then react with this radical site, forming a hydroxyl group.

The detachment of the oleoyl chain can give rise to structural disintegration (possibly leading to pore formation) or to a change in the fluidity of the PLB. This behavior cannot be studied with the DFTB method, which is too computationally intensive, but in the next section, we will illustrate such a mechanism, which occurs on the ns time scale, by means of united-atom non-reactive MD simulations.

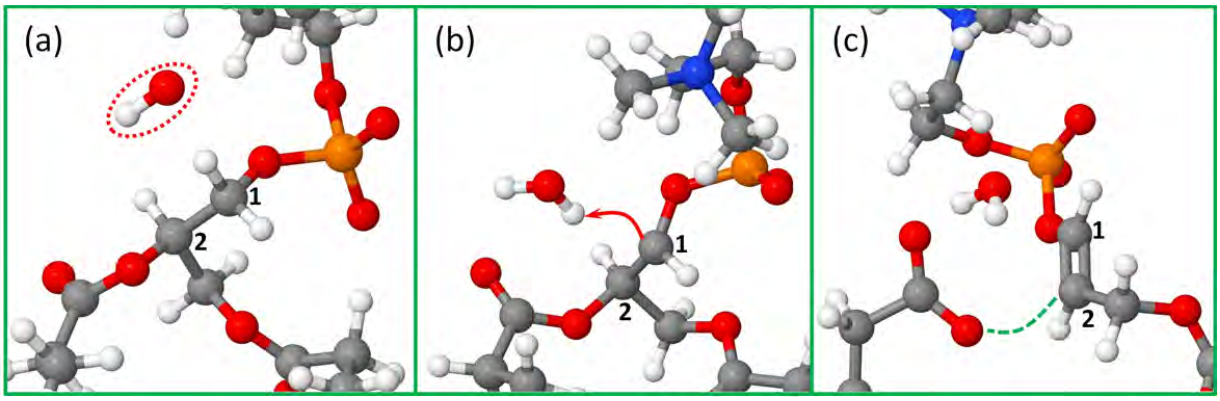

Figure 14: Snapshots from the DFTB-MD simulations, illustrating the breaking mechanism of a C-O bond upon impact of an OH radical. The OH radical (shown in red dashed circle) approaches the H atom connected to C_1 (a), and abstracts it, leading to the formation of a water molecule (b). This results in the formation of a double C_1=C_2 bond and the cleavage of a C-O bond (c), leading to the detachment of the oleoyl fatty acid tail (cf. Figure 12(a)). The H-abstraction and the dissociation of the bond are indicated in the figure with a red arrow and a green dashed line, respectively. The color legend is identical to Figure 12.

3.6. Phospholipid bilayer: United atom non-reactive MD study

(a) Computational details

Finally, to investigate the effect of lipid peroxidation products on the structural and dynamic properties (i.e., fluidity and permeability) of the plasma membrane, we carried out non-reactive united-atom MD simulations. Although a plasma membrane consists of both lipids and proteins, which both contribute for about 50% to the mass of the plasma membrane, our model system only considers the lipids, as they play a crucial role in the structure of the bilayer.

As input structures, we are not yet able to use the structures obtained by lipid peroxidation in previous section, but we constructed some model systems, based on literature data for lipid peroxidation products [115]. Our model systems contain 72 lipids. We investigated two types of lipid systems. The first type is all made of POPC (cf. previous section). This phospholipid forms a large fraction of the lipids

in the plasma membrane [116]. The second type also contains cholesterol (up to 50% molar fraction), besides the POPC lipids. This allows us to investigate the difference between cancer cells and healthy cells. Indeed, it is known that cancer cells have a significantly lower concentration of cholesterol in their plasma membrane [117].

To study the effect of lipid peroxidation, we added lipid peroxidation products to the above model systems, with concentrations varying between 0 and 100%, keeping the total number of lipids (i.e., POPC, cholesterol and lipid peroxidation products) equal to 72. Although several different lipid peroxidation products might occur, we focus on two different types, which are frequently observed as reaction products [115], i.e., a simple peroxide of POPC, as well as two aldehydes, formed by a ring-forming – ring-opening reaction of a peroxyl radical of POPC. These products, as well as POPC, are illustrated in Figure 15. Note that we do not consider peroxidation products of cholesterol, as the peroxidation of cholesterol is much slower than for unsaturated phospholipids [118]. Moreover, the oxidation products of cholesterol still contain rigid ring structures, so we can expect that even upon oxidation, the effect on the structure of the bilayer will be limited.

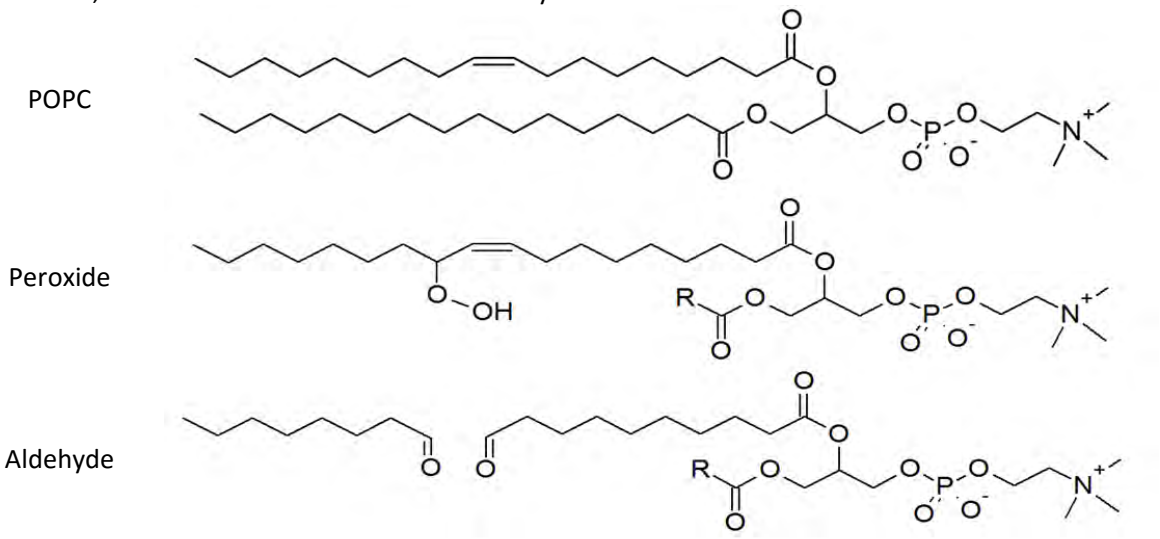

Figure 15: Schematic representation of POPC and the two peroxidation products considered (peroxide and aldehyde).

In total, we thus consider 32 model systems. Finally, besides the 72 lipids, the system also contains 4000 water molecules, all positioned in a box of about 5.5nm x 5.5nm x 11nm. An example of a model structure, containing 36 POPC molecules and 36 cholesterol molecules, surrounded by water molecules at both sides of the lipid bilayer, is presented in Figure 16.

As mentioned above, we make use of united-atom non-reactive MD simulations, which allow to handle time-scales up to hundreds of nanoseconds. This is needed to be able to observe pore formation in the plasma membrane, which occurs at a time-scale of several ns. As mentioned in section 2, the united-atom approach does not treat all atoms in the system individually, but it combines the C-atoms and H-atoms bonded to it into one group, i.e., the methyl or methylene groups in the lipid tails. In polar bonds, like in a hydroxyl group or in water molecules, however, the H-atoms remain as separate atoms, which allows to explicitly study the effect of lipid peroxidation products. The POPC molecule in the model system, which consists of 134 atoms, can in this way be reduced to a system of 52 particles.

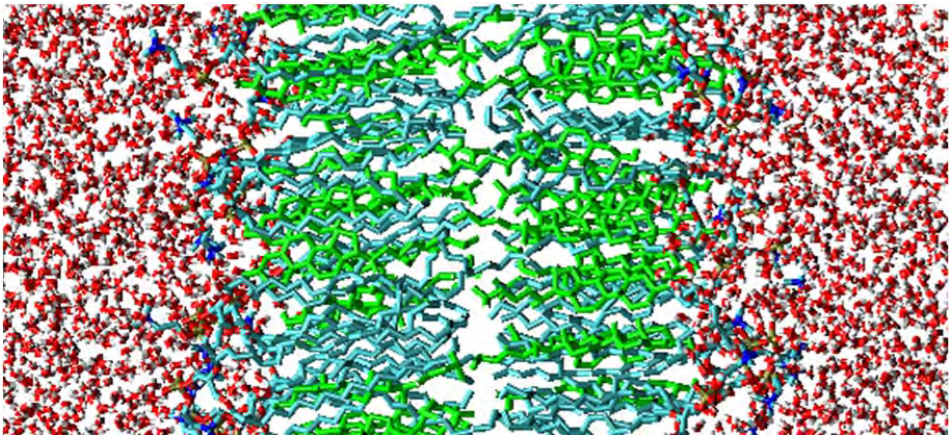

Figure 16: Snapshot of the structure of a bilayer containing 36 POPC molecules and 36 cholesterol molecules. Red parts represent oxygen, white parts hydrogen, dark blue represents nitrogen, while cyan represents carbon, tan parts represent phosphorus and cholesterol is entirely coloured in green.

The model systems are constructed by randomly placing the various lipids in the simulation box, keeping the atoms of different lipids at a minimum distance of 2 Å from each other, to avoid unrealistically large forces at the start of the MD simulation. To obtain this initial configuration, the Packmol package was used [119]. As a result, the initial structure is far from the optimal equilibrium structure, so we first need to perform an energy minimization, using the steepest decent algorithm, followed by an equilibration in the NPT-ensemble. The temperature is kept constant by the Nosé-Hoover thermostat at a reference temperature of 303 K and a coupling constant of 0.2 ps [120]. The pressure is controlled by the semi-isotropic Parinello-Rahman coupling scheme, with a reference pressure of 1 atm, a compressibility of 4.5×10^{-5} bar^{-1}, and a coupling constant of 1 ps. Periodic boundary conditions in all three dimensions are applied.

We apply the GROMOS 43A1-S3 force field [70], which contains parameters for a wide variety of lipids, including cholesterol, but not for the peroxide and aldehyde groups considered in this study. Therefore,

we have implemented them from literature [71]. A time-step of 2 fs is used for the MD simulations, and in total 40 million iterations are performed, yielding a total simulated time of 80 ns. The geometry of the system is recorded after each 100 ps, to average the output of the simulations for the further analysis.

The effects of the lipid peroxidation products are investigated by analyzing some typical properties of lipid bilayers, i.e., the surface area per lipid, the thickness of the bilayer, the water density inside the bilayer (used as a measure for the polarity inside the membrane), and the so-called deuterium order parameter, which is a measure for the order of the lipid tails in the bilayer.

(b) Illustration of results

Figure 17 presents the surface area per lipid (a), the thickness of the bilayer (b), the water density inside the bilayer (c) and the deuterium order parameter (d), for the model system without cholesterol, as a function of the concentration of the oxidized phospholipids, for both the peroxide and the aldehydes. It is clear that the surface area per lipid (Figure 17(a)) increases upon oxidation, in agreement with experimental and computational observations from literature [71,72,121]. This can be explained because the polar groups formed after oxidation (peroxide or aldehydes) prefer to move towards the water layer, to maximize their interactions with the water molecules. This bended conformation results in a larger surface area within the membrane. The effect is slightly larger for the aldehydes, because of the two shorter chains, having a higher mobility, and thus allowing to change the conformation more easily.

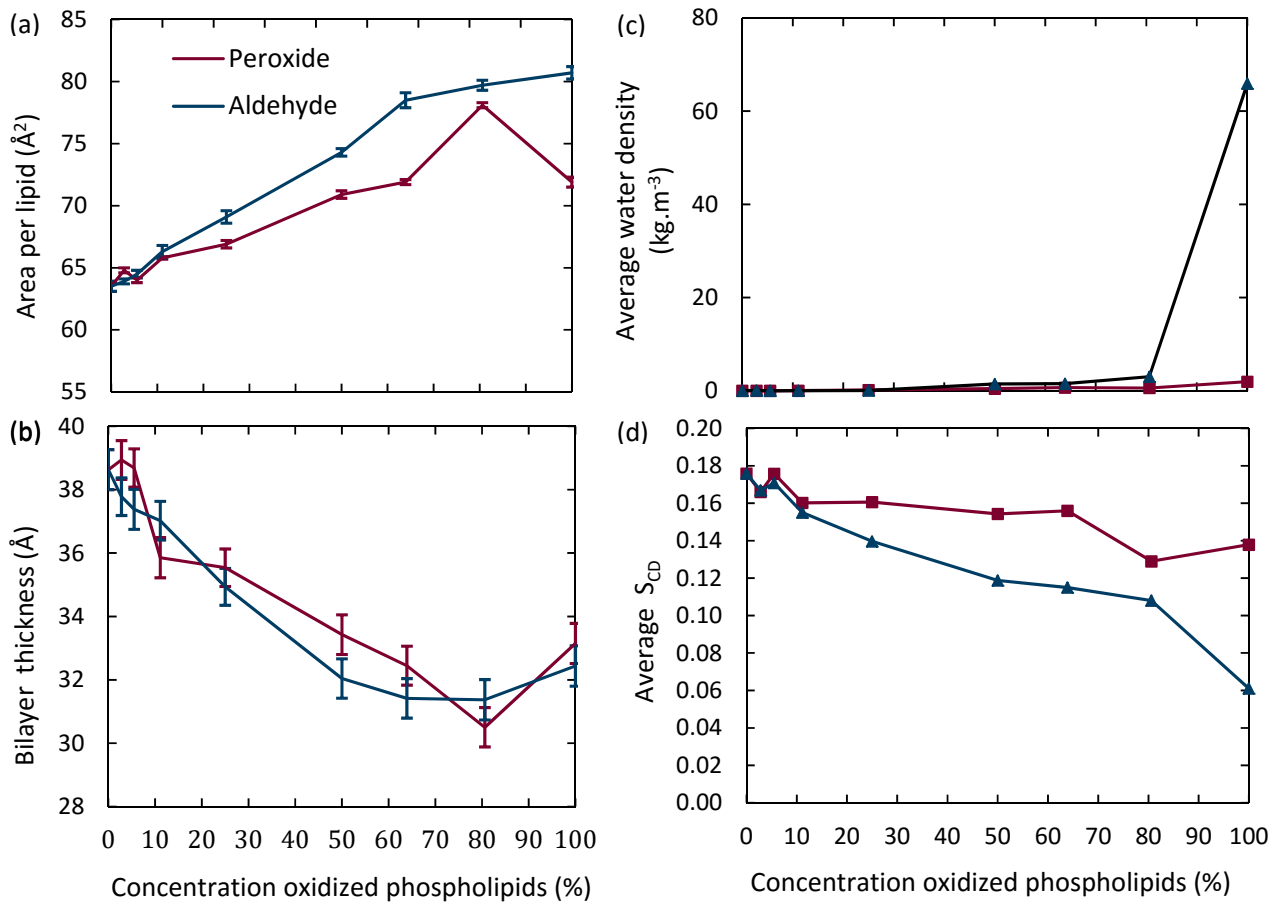

Figure 17: Surface area per lipid (a), thickness of the bilayer (b), average water density in the center of the bilayer (c) and average deuterium order parameter (d), as a function of the concentration of the oxidized phospholipids, for two types of oxidation products, for the model system without cholesterol.

The thickness of the bilayer generally drops upon oxidation, as is clear from Figure 17(b). This is directly linked to the rise in surface area per lipid, because the lipid bilayer can in first instance be considered as a non-compressible fluid with constant volume. Note that the effect of plasma treatment on a phospholipid bilayer can be investigated by Raman microscopy and dynamic light scattering, as well as by X-ray measurements of the bilayer electron density (to study the modification in bilayer thickness) or by the Laurdan Assay method (to study the lipid rigidization or fluidization), as demonstrated already by Hammer et al. [16,122], who found that plasma treatment yields increased fluidity of the lipid bilayer. It would be very interesting to validate our model calculations in detail with such type of measurements.

It is interesting to note that for oxidation approaching 100%, the double layer thickness rises again. This is attributed to pore formation, as is illustrated in Figure 18 for the aldehyde oxidation products. Figure 18(a) represents the initial conformation (after 10 ns), without water defects. After 60 ns (Figure 18(b)), a significant amount of water has moved into the center of the bilayer, and after 120 ns (Figure 18(c)), a pore with diameter of 15 Å is formed. This pore size is too small to allow the migration of entire organelles or macromolecules, e.g. proteins, through the membrane, which might explain why typically apoptosis instead of necrosis is observed [123]. Plasma species, like RONS, are however small enough to migrate through the membrane. The thickness of the double layer is also indicated in Figure 18. The pore formation allows water to enter the bilayer, resulting in swelling, and hence a thicker bilayer. This pore formation is in agreement with literature observations for a similar oxidation product as the aldehydes studied here [74].

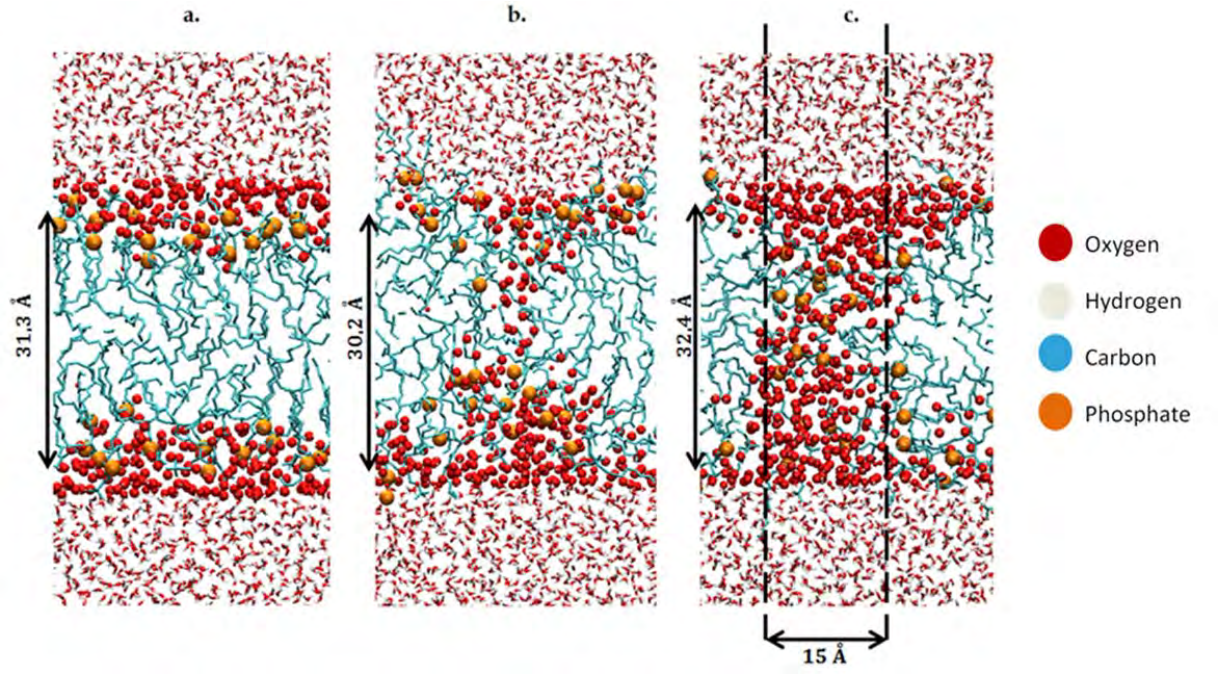

Figure 18: Snapshot of the MD simulations, for a time of 10 ns (a), 60 ns (b) and 120 ns (c), illustrating the pore formation, in the model system without cholesterol and 100% oxidation to aldehydes.

The fact that in the case of 100% oxidation to aldehydes a significant amount of water can move through the membrane, while this is not (yet) observed for the peroxide, is also clear from Figure 17(c),

illustrating the water density in the center of the bilayer upon oxidation, for both oxidation products. It is clear that even 80% oxidation to the aldehydes has a negligible effect on the water density, but a higher oxidation degree leads to a significant rise, corresponding to the pore formation.

Finally, the deuterium order parameter is plotted against oxidation degree in Figure 17(d). A drop in the order of the lipid tails is observed, because the polar groups yield a distortion in the apolar environment, and the effect is more pronounced for the aldehydes, because of the shorter chain lengths. In general, we can conclude that the bilayer becomes more fluid upon oxidation, which can finally lead to pore formation.

The above results were obtained for the model systems without cholesterol. We also performed calculations with model systems including cholesterol, and the results indicate that the cell membrane fluidity does not increase to the same extent, and no pore formation is observed. Figure 19 illustrates the water density in the center of the bilayer in the case of 100% oxidation to aldehydes, upon increasing fraction of cholesterol in the bilayer. The significant water density in case of a cholesterol concentration up to 11.1% indicates the occurrence of pore formation, but a higher cholesterol concentration yields a significant drop in water density, meaning that pore formation is inhibited. This finding is important for cancer treatment by plasma, as cancer cells contain far less cholesterol than their healthy counterparts (see above). Thus, they might be far more prone to the penetration of ROS produced by plasma in the interior of the cell, giving rise to oxidative stress, inducing pro-apoptotic factors, and this might explain why plasma can selectively treat cancer cells, while leaving their healthy counterparts undamaged.

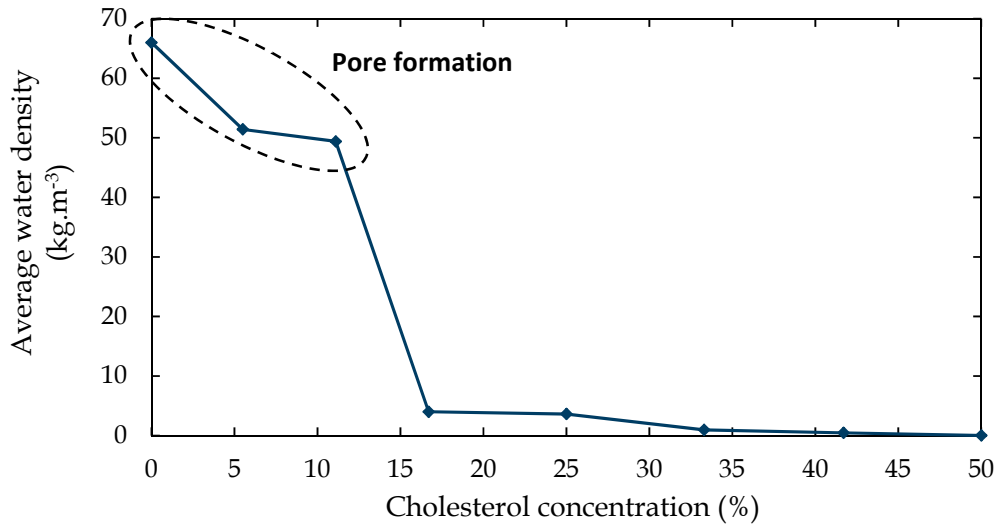

Figure 19: Average water density in the center of the bilayer, for the model systems with 100% oxidation to aldehydes, as a function of cholesterol concentration in the bilayer.

4. Summary and Conclusions

In this paper, we gave an overview of the different atomic/molecular level computational methods, that can be applied in the context of plasma medicine for studying plasma-biomolecule interactions. To demonstrate the capabilities and limitations of the various methods, we have applied them to three important groups of biomolecular systems, i.e., proteins, DNA and a phospholipid bilayer.

The QM/MM method was applied to a very simple peptide model system (deca-alanine), showing the potential of this method for a very accurate description of chemical reactions at important reactive sites of biomolecules, whereas the rest of the biomolecule and the surrounding water molecules can be treated in a non-reactive way, while still accounting for their influence on the reactive site. This method allows to treat model systems up to a few 100,000 atoms, with typically about 100 atoms in the QM part, for time scales in the order of picoseconds.

Another QM method with great potential to describe the interaction of ROS with biomolecules is DFTB, which is an approximate DFT method. It was applied here to study the interaction of OH radicals with P-glycoprotein (more specifically with the TM6 domain), a transmembrane protein playing a crucial role in drug binding in human cells. This model system contains 326 atoms, and it can be treated with DFTB on a time scale of tens of picoseconds. Our simulations reveal that OH radicals can react with the backbone and side chains of this protein domain (TM6), leading to oxidation, peptide fragmentation and even mutation. To study the long-term effect of this mutation on the structure of TM6, we also performed non-reactive MD simulations. The model system was the same (i.e., 326 atoms), but the time scale could be extended to a few 100 ns. The results clearly indicate that TM6 becomes less flexible upon this mutation, and we expect that this will affect the drug binding affinity of P-glycoprotein. This suggests that plasma therapy (or other therapies based on ROS) may provide a solution to the resistance of cancer cells against chemotherapy, and thus contribute to a better cancer treatment in combination with classical (chemo)therapies. However, further research will be needed to investigate in more detail the drug binding affinity of the native and mutant structures of TM6 of P-glycoprotein.

Furthermore, we have also applied classical reactive MD simulations based on the Reax force field to study the interaction of OH radicals with part of a DNA molecule. Depending on the complexity of the force field, this method can handle a few 10,000 to several 100,000 atoms at a time scale up to tens of ns. Our calculations have provided atomic scale insight in the oxidative stress on DNA, caused by OH radicals. Important processes are among others the first steps towards the formation of 8-oxo-guanine and 8-oxo-adenine, which form the markers for oxidative stress on cells and are able to trigger apoptosis, as often seen experimentally.

The DFTB method was also used to investigate the interaction of OH radicals with a PLB, elucidating the underlying mechanisms of lipid (per)oxidation. This model system contains 1915 atoms, which is considerable for an (approximate) QM method, and was treated on a time scale of 5 ps. Moreover, the long-term effect of the PLB after lipid (per)oxidation was studied with classical non-reactive united-atom MD simulations. This method allows to predict whether the reactions of plasma species with the cell membrane, typically leading to (per)oxidation, can give rise to structural disintegration (e.g., pore formation), allowing ROS from the plasma to penetrate through the plasma membrane. This model system contains 72 lipids, as well as 4000 water molecules, corresponding to about 15,000 particles, or 20,000 real atoms, and can be followed over a time scale of several 100 ns. Our simulations indeed reveal that the fluidity of a phospholipid bilayer, as a model system for the plasma membrane, increases when it contains a higher fraction of lipid peroxidation products. Eventually, when all phospholipids are peroxidized, pore formation was observed. On the other hand, when the phospholipid bilayer also contains cholesterol molecules, the plasma membrane fluidity seems not to increase to the same extent, and pore formation did not occur. As the plasma membrane of cancer cells contains far less cholesterol than their healthy counterparts, these results suggest that ROS from the plasma can more easily penetrate the plasma membrane of cancer cells, giving rise to oxidative stress, and this might be one of the reasons why plasma can selectively treat cancer cells.

These examples illustrate the strengths and limitations of the various methods. As with every type of model, the accuracy of the different methods crucially depends on the accuracy of the input data. Of the

methods described in this paper, DFT is the most accurate. Note, however, that also in this case, the accuracy strongly depends on the applied functional. Moreover, due to the high computational cost, DFT can typically only describe very small systems (i.e., usually in the order of 100 atoms, over a time scale of picoseconds, when used in an MD setup). This condition can be somewhat relaxed when integrating DFT into a QM/MM setup, treating only the active site with DFT and the rest of the biomolecule with the MM method. This allows to treat larger systems (i.e., a few 100,000 atoms, as determined by the MM part), but the time scale remains to be determined by the QM method. DFTB is an approximate DFT method, and the accuracy depends on the level of theory used and on the input parameters. Our experience, based on the SCC-DFTB method, is quite positive. Indeed, our results obtained by this method appear to be realistic, as far as they can be validated by (more accurate QM or experimental) data from literature. The DFTB method can treat a few thousand atoms on a time scale of tens of picoseconds. This method is thus about two orders of magnitude faster than DFT, but we experienced that DFTB-based MD simulations are still ~50 times slower than ReaxFF-based MD simulations. On the other hand, the accuracy of the ReaxFF-based MD simulations also critically depends on the force field used, and in our experience, this force field is not always accurate enough; this sometimes yields unrealistic results. Hence, this method needs to be used with caution. Finally, non-reactive MD simulations cannot describe bond breaking and formation, and they are thus not able to study chemical reactions of plasma species with biomolecules. Nevertheless, they are very powerful for describing very large biomolecular systems (containing millions of atoms and even more) after ROS impacts, on a longer time scale (i.e., a few 100 ns), which is not accessible by reactive MD simulations. This is even more true for united-atom non-reactive MD simulations, which can simulate even larger systems (order of tens of millions of particles), again on a time scale of a few 100 ns. This allows to study pore formation in a phospholipid bilayer, after ROS-induced lipid (per)oxidation. The latter is of great interest in the context of plasma medicine (or other therapies based on ROS). Finally, it is worth to mention that record MD simulations even go beyond those scales, containing up to 10^{12} atoms (albeit using a simple Lennard-Jones potential) [124], and time scales up to milliseconds (albeit for much smaller systems) [125].

In general, we can conclude that, in order to obtain a global picture of the various processes playing a role in plasma-biomolecule interactions, a multi-level approach is most appropriate, as the combination of the above methods enables to describe not only the processes occurring during the interaction of the plasma species with biomolecules, but also the long-term behavior after these interactions. However, it is clear that these simulations only provide some insight in the first step processes of plasma medicine. Indeed, plasma medicine is quite complicated, due to the complex nature of living cells. Processes like cell signaling and systemic reactions are clearly beyond the scope of the present type of simulations.

Acknowledgements

This work is financially supported by the Fund for Scientific Research Flanders (FWO) and the Francqui Foundation. The calculations were carried out in part using the Turing HPC infrastructure of the CalcUA core facility of the Universiteit Antwerpen, a division of the Flemish Supercomputer Center VSC, funded by the Hercules Foundation, the Flemish Government (department EWI) and the Universiteit Antwerpen.

References

1. Neyts E C, Yusupov M, Verlackt C C and Bogaerts A 2014 *J. Phys. D: Appl. Phys.***47** 293001

2. Yusupov M, Neyts E C, Khalilov U, Snoeckx R, van Duin A C T and Bogaerts A 2012 *New J. Phys.* **14** 093043
3. Yusupov M, Bogaerts A, Huygh S, Snoeckx R, van Duin A C T and Neyts E C 2013 *J. Phys. Chem.* C **117** 5993
4. Yusupov M, Neyts E C, Verlackt C C, Khalilov U, van Duin A C T and Bogaerts A 2015 *Plasma Process. Polym.* **12** 162
5. Yusupov M, Neyts E C, Simon P, Bergiyorov G, Snoeckx R, van Duin A C T and Bogaerts A 2014 *J. Phys. D: Appl. Phys.* **47** 025205
6. Lackmann J-W, Schneider S, Edengeiser E, Jarzina F, Brinckmann S, Steinborn E, Havenith M, Benedikt J and Bandow J E 2013 *J R Soc Interface* **10** 20130591
7. Chung T-Y, Ning N, Chu J W, Graves D B, Bartis E, Seog J and Oehrlein G S 2013 *Plasma Process. Polym.* **10** 167
8. Bartis E A J, Graves D B, Seog J and Oehrlein G S 2013 *J. Phys. D: Appl. Phys.* **46** 312002
9. Bartis E A J, Barrett C, Chung T Y, Ning N, Chu J W, Graves D B, Seog J and Oehrlein G S 2014 *J. Phys. D: Appl. Phys.* **47** 045202
10. Park J H, Kumar N, Park D H, Yusupov M, Neyts E C, Verlackt C C W, Bogaerts A, Kang M H, Uhm H S, Choi E H and Attri P 2015 *Sci. Reports* **5** 13849
11. Marschewski M, Hirschberg J, Omairi T, Hofft O, Viol W, Emmert S and Maus-Friedrichs W 2012 *Exp Dermatol* **21** 921
12. Takai E, Kitamura T, Kuwabara J, Ikawa S, Yoshizawa S, Shiraki K, Kawasaki H, Arakawa R and Kitano, K 2014 *J. Phys. D: Appl. Phys.* **47** 285403
13. Madugundu G S, Cadet J and Wagner J R 2014 *Nucleic Acids Research* **42** 7450
14. Hong S-H, Szili E J, Jenkins A T A and Short R D, 2014 *J. Phys. D: Appl. Phys.* **47** 362001
15. Szili E J, Bradley J W and Short R D, 2014 *J. Phys. D: Appl. Phys.* **47** 152002
16. Hammer M U, Forbrig E, Kupsch S, Weltmann K-D and Reuter S 2013 *Plasma Medicine* **3** 97
17. Echenique P and Alonso J L 2007 *Mol. Phys*. **105** 3057
18. Cremer D 2011 *WIREs Comput. Mol. Sci*. **1** 509
19. Bartlett R J, Musial M 2007 *Rev. Mod. Phys*. **79** 291
20. Sherrill C D and Schaefer III H F 1999 *Adv. Quantum Chem*. **34** 143
21. Parr R G and Yang W 1995 *Annu. Rev. Phys. Chem*. **46** 701
22. Hohenberg P and Kohn W 1964 *Phys. Rev.* **136**B864
23. Perdew J P, in *Electronic structure of solids '91*, Eds. P. Ziesche, H. Eschrig, Akademie Verlag, Berlin, 1991, 11
24. Perdew J P and Wang Y 1992 *Phys. Rev. B***45** 13244
25. Perdew J P, Burke K and Ernzerhof M 1996 *Phys. Rev. Lett*. **77** 3865
26. Perdew J P, Burke K and Ernzerhof M 1997 *Phys. Rev. Lett*. **78** 1396
27. Becke A D 1993 *J. Chem. Phys*. **98** 5648
28. Lee C, Yang W and Parr R G 1988 *Phys. Rev. B* **37** 785
29. Barnett R N and Landman U 1993 *Phys. Rev. B***48** 2081
30. Car R and Parrinello M 1985 *Phys. Rev. Lett*. **55** 2471
31. Galano A, Alvarez-Idaboy J R, Montero L A and Vivier–Bunge A 2001 *J. Comput. Chem*. **22** 1138
32. Galano A and Cruz-Torres A 2008 *Organ. & Biomolec. Chem*. **6** 732
33. Huang M L and Rauk A 2004 *J. Phys. Organ. Chem*. **17** 777
34. Scheiner S and Kar T 2010 *J. Am. Chem. Soc*. **132** 16450
35. Georgieva P and Himo F 2008 *Chem. Phys. Lett*. **463** 214
36. Natsume T, Ishikawa Y, Dedachi K, Tsukamoto T and Kurita N 2006 *Int. J. Quantum Chem*. **106** 3278
37. Shimizu E, Hoshino R, Nomura K, Danilov V I and Kurita N 2013*J. Mod. Phys*. **4** 442

38. Jolibois F, Soubias O, Réat V and Milon A 2004 *Chemistry* **10** 5996
39. Solis-Calero C, Ortega-Castro J and Muños F 2010 *J. Phys. Chem. B* **114** 15879
40. Krishnamurty S, Stefanov M, Mineva T, Bégu S, Devoisselle J M, Goursot A, Zhu R and Salahub D R 2008 *J. Phys. Chem. B* **112** 13433
41. Porezag D, Frauenheim Th., Köhler Th, Seifert G and Kaschner R 1995*Phys. Rev. B***51** 12947
42. Elstner M, Porezag D, Jungnickel G, Elsner J, Haugk M, Frauenheim Th, Suhai S and Seifert G 1998*Phys. Rev. B***58** 7260
43. Liang R, Swanson J M J and Voth G A 2014*J. Chem. Theory Comput*. **10** 451
44. Elstner M 2006*Theor. Chem. Acc*. **116** 316
45. Han W-G, Elstner M, Jalkanen K J, Frauenheim Th and Suhai S 2000*Int. J. Quantum Chem*. **78** 459
46. Elstner M, Frauenheim Th and Suhai S 2003 *THEOCHEM* **632** 29
47. Elstner M, Hobza P, Frauenheim Th, Suhai S and Kaxiras E 2001 *J. Chem. Phys*. **114** 5149
48. Shishkin O V, Elstner M, Frauenheim Th, Suhai S 2003 *Int. J. Molec. Sci*. 4 537
49. Gaus M, Goez A andElstner M 2013 *J. Chem. Theory Comput*. **9** 338
50. Babaeva N Y, Ning N, Graves D B and Kushner M J 2012 *J. Phys. D: Appl. Phys.* **45** 115203
51. Van der Paal J, Aernouts S, van Duin A C T, Neyts E C and Bogaerts A 2013 *J. Phys. D: Appl. Phys.* **46** 395201
52. Van der Paal J, Verlackt C C, Yusupov M, Neyts E C and Bogaerts A 2015 *J. Phys. D: Appl. Phys.***48** 155202
53. Abolfath R M, van Duin A C T and Brabec T 2011 *J. Phys. Chem.* A **115** 11045
54. Abolfath R M, Biswas P K, Rajnarayanam R, Brabec T, Kodym R and Papiez L 2012 *J. Phys. Chem.* A **116** 3940
55. Khosravian N, Bogaerts A, Huygh S, Yusupov M and Neyts E C 2015 *Biointerphases* **10** 029501
56. Brenner D W 1990 *Phys. Rev. B* **42** 9458
57. vanDuin A C T, Dasgupta S, Lorant F and Goddard W A III 2001 *J. Phys. Chem.* A **105** 9396
58. Cornell W D, Cieplak P, Bayly C I, Gould I R, Merz K M Jr, Ferguson D M, Spellmeyer D C, Fox T, Caldwell J W and Kollman P A 1995 *J. Am. Chem. Soc*. **117** 5179
59. Vanommeslaeghe K, Hatcher E, Acharya C, Kundu S, Zhong S, Shim J, Darian E, Guvench O, Lopes P, Vorobyov I and MacKerell A D Jr 2010 *J. Comput. Chem*. **31** 671
60. Yu W, He X, Vanommeslaeghe K and MacKerell A D Jr 2012 *J. Comput. Chem*. **33** 2451
61. van Gunsteren W F and Berendsen H J C, *Groningen Molecular Simulation (GROMOS) Library Manual,* Biomos, Groningen, The Netherlands, 1987, pp. 1-221
62. van Gunsteren W F, Billeter S R, Eising A A, Hünenberger P H, Krüger P, Mark A E, Scott W R P and Tironi I G, *Biomolecular Simulation: The GROMOS96 Manual and User Guide,* Vdf Hochschulverlag AG an der ETH Zürich, Zürich, Switzerland, 1996, pp. 1-1042
63. Borhani D W, Shaw D E 2012 *J. Computer-Aided Molecul. Design* 26 15
64. Durrant J D and McCammon J A 2011 *BMC biology* 9 71
65. Chadha N, Tiwari A K, Kumar V, Milton M D, Mishra A K 2015 *J. Biomolec. Struct. Dynam.* 33 573
66. Cole D J, Tirado-Rives J and Jorgensen W L 2015 *Biochim. Biophys. Acta*1850 966
67. Mortier J, Rakers C, Bermudez M, Murgueitio M S, Riniker S, Wolber G 2015 *Drug discovery Today* 20 686
68. Marrink S J, Risselada H J, Yefimov S, Tieleman D P and De Vries A H 2007 *J. Phys. Chem. B***111** 7812
69. Berger O, Edholm O and Jahnig F 2013 *Biophys. J.* **72** 2002
70. Chiu S W, Pandit S A, Scott H L and Jakobsson E 2009 *J. Phys. Chem. B* **113** 2748
71. Wong-Ekkabut J, Xu Z, Triampo W, Tang I-M, Tieleman D P and Monticelli L 2007 *Biophys. J.* **93** 4225

72. Jurkiewicz P, Olzyńska A, Cwiklik L, Conte E, Jungwirth P, Megli F M and Hof M 2012 *Biochim. Biophys. Acta - Biomembr.* **1818** 2388
73. Khandelia H and Mouritsen O G 2009 *Biophys. J.* **96** 2734
74. Cwiklik L and Jungwirth P 2010 *Chem. Phys. Lett.* **486** 99
75. Beranova L, Cwiklik L, Jurkiewicz P, Hof M and Jungwirth P 2010 *Langmuir* **26** 6140
76. Baaden M and Marrink S J 2013 *Current Opinion in Struct. Biol*. **23** 878
77. Periole X, Huber T, Marrink S J and Sakmar T P2007*J. Am. Chem. Soc*. **129** 10126
78. Parton D L, Klingelhoefer J W and Sansom M S P 2011 *Biophys. J.* **101** 691
79. Savelyev A and Papoian G A 2010 *Proc. Nat. Acad. Sci*. **107** 20340
80. Cao Q, Zuo C, Ma Y, Li L and Zhang Z 2011 *Soft Matter* **7** 506
81. Palleschi A, Bocchinfuso G, Coviello T and Alhaique E 2005 *Carbohydr. Res*. **340** 2154
82. Zhang Q, Bulone V, Agren H and Tu Y 2011 *Cellulose* **18** 207
83. Field M J, Bash P A and Karplus M 1990 *J. Comput. Chem*. **11** 700
84. Åqvist J and Warshel A 1993 *Chem.Rev*. **93** 2523
85. Gao J 1996 *Accounts Chem.Res*. **29** 298
86. Dewar M J, Zoebisch E G, Healy E F and Stewart J J 1985 *J. Am. Chem. Soc*.**107**3902
87. Stewart J J 1990 *J.Computer-aided Molec. Design* **4**1
88. Hwang J K, King G, Creighton S and Warshel A 1988*J. Am. Chem. Soc*. **110** 5297
89. Parr R G1983 *Annual Rev. Phys. Chem*. **34** 631
90. Senn H M and Thiel W 2009 *Angew. Chemie Int. Ed*. **48** 1198
91. Brooks B R, Brooks C L, MacKerell A D, Nilsson L, Petrella R J, Roux B, Won Y, Archontis G, Bartels C and Boresch S 2009 *J.Comput.Chem*. **30** 1545
92. Humbel S, Sieber S and Morokuma K 1996 *J.Chem.Phys*. **105** 1959
93. Ambudkar S V, Kimchi-Sarfaty C, Sauna Z E and Gottesman M M 2003 *Oncogene* **22** 7468
94. Longley D and Johnston P 2005 *J. Pathol.* **205** 275
95. Loo T and Clarke D 2005 *J. Membr. Biol*. **206** 173
96. Loo T W and Clarke D M 1994 *Biochem*. **33** 14049
97. Maskos Z, Rush J and Koppenol W 1992 *Archives Biochem. Biophys*. **296** 521
98. Köritzer J, Boxhammer V, Schäfer A, Shimizu T, Klämpfl T G, Li Y-F, Welz C, Schwenk-Zieger S, Morfill G E, Zimmermann J L, Schlegel J 2013 *PLOS One* **8** e64498
99. Hess B, Kutzner C, Van Der Spoel D and Lindahl E 2008 *J. Chem. Theory Comput*. **4** 435
100. Cheatham T E III, Miller J L, Fox T Darden T A, Kollman P A 1995 *J. Am. Chem. Soc*. **117** 4193
101. Monti S, Corozzi A, Fristrup P, Joshi K L, Shin Y K, Oelschlaeger P, van Duin A C T and Barone V 2013 *Phys. Chem. Chem. Phys*. **15** 15062
102. Dizdaroglu M and Jaruga P 2012 *Free Radic. Res*. **46** 382
103. Cadet J, Douki T, Ravanat J-L and Di Mascio P 2009 *Photochem. Photobiol. Sci*. **8** 903
104. Jena N R and Mishra P C 2005 *J. Phys. Chem. B* **109** 14205
105. Shao C, Saito M and Yu Z 1999 *Radiat. Environm. Biophys.***38** 105
106. Verlackt C C W, Neyts E C, Jacob T, Fantauzzi D, Golkaram M, Shin Y-K, van Duin A C T and Bogaerts A 2015 *New J. Phys.* (in press).
107. Alberts B,Johnson A, Lewis J, Raff M, Roberts K and Walter P2010 *Molecular Biology of the Cell, Classic textbook 5th Ed.* (New York: Garland Science)
108. Berendsen H J C, Postma J P M, van Gunsteren W F, DiNola A and Haak J R 1984 *J. Chem. Phys.* **81** 3684
109. Niki E, Yoshida Y, Saito Y and Noguchi N 2005 *Biochem. Biophys. Res. Commun.* **338** 668
110. Catala A 2009 *Chem. Phys. Lipids* **157** 1
111. Catala A 2010 *Biochem. Biophys. Res. Commun.* **399** 318
112. Cordeiro R M 2014 *Biochim. Biophys.* **1838** 438

113. Stephens P J,Devlin F J, Chabalowski C F and Frisch M J 1994*J. Phys. Chem.* **98** 11623
114. van Lenthe E and Baerends E J 2003 *J. Comput. Chem*. **24** 1142
115. Reis A, Domingues M R M, Amado F M L, Ferrer-Correia a. J V and Domingues P 2005 *Biomed. Chromatogr.* **19** 129
116. Spector A A and Yorek M A 1985 *J. Lipid Res*. **26** 1015
117. Van Blitterswijk J W, De Veer G, Krol H J and Emmelot P 1982 *Biochim. Biophys.Acta* **688** 495
118. Schnitzer E, Pinchuk I, Bor A, Leikin-Frenkel A and Lichtenberg D 2007 *Chem. Phys. Lipids* **146** 43
119. Martinez L, Andrade R, Birgin E G and Martinez J M 2009 *J. Comput. Chem.* **30** 2157
120. Hoover G W 1985 *Phys. Rev.* **31** 1695
121. Lis M, Wizert A, Przybylo M, Langner M, Swiatek J, Jungwirth P and Cwiklik L 2011 *Phys. Chem. Chem. Phys.* **13** 17555
122. Hammer M U, Kupsch S, Forbrig E, Tresp H, Masur K, Weltmann K -D, Beerlink A, Gutsmann T and Reuter S, *Influence of plasma-treated liquids on structure and function of lipid membranes,* Poster presentation at the 5th International Conference on Plasma Medicine (ICPM5), May 18-23, **2014**, Nara, Japan
123. Fridman G, Shereshevsky A, Jost M M, Brooks A D, Fridman A, Gutsol A, Vasilets V and Friedman G 2007 *Plasma Chem. Plasma Process.* **27** 163
124. Germann T C and Kadau K 2008 *Int. J. Mod. Phys. C* **19** 1315
125. Voelz V A, Bowman G R, Beauchamp K and Pande V S 2010 *J. Am. Chem. Soc.* **132** 1526